Supporting Informations for

Isotopically Enriched Polymorphs of Dysprosium Single Molecule Magnets

Yosuke Kishi,[a,b] Fabrice Pointillart,*[b] Bertrand Lefeuvre,[b] François Riobé,[c] Boris Le Guennic,[b] Stéphane Golhen,[b] Olivier Cador,*[b] Olivier Maury,[c] Hideki Fujiwara,*[a] Lahcène Ouahab[b]

[a] *Department of Chemistry, Graduate School of Science, Osaka Prefecture University, 1-1 Gakuen-cho, Naka-ku, Sakai, Osaka*
599-8531, Japan

[b] *Institut des Sciences Chimiques de Rennes UMR 6226 CNRS-UR1, Université de Rennes 1, 35042 Rennes Cedex, France.*

[c] *Laboratoire de Chimie de l'ENS-LYON-UMR 5182, 46 Allée d'Italie, 69364 Lyon Cedex 07.*

Corresponding author's email: fabrice.pointillart@univ-rennes1.fr, Olivier.cador@univ-rennes1.fr, hfuji@c.s.osakafu-u.ac.jp

Experimental Section

General Procedures and Materials. The precursors $Ln(tta)_3{\cdot}2H_2O$ (Ln=Eu^{III}, Dy^{III}, Er^{III} and Yb^{III}; tta^-=2-thenoyltrifluoroacetonate anion)1, $^{164}Dy(tta)_3{\cdot}2H_2O$,47 4,5-bis(methylthio)tetrathiafulvalene[2] and 2-(5-bromopyridin-2-yl)-1,3-benzothiazole[3,4] were synthesized following previously reported methods. All other reagents were purchased from Aldrich Co., Ltd. and used without further purification.

Synthesis of 4-[6-(1,3-benzothiazol-2-yl)pyridin-3-yl]-4',5'-bis(methylthio)tetrathiafulvene (L). To a stirred solution of 4,5-bis(methylthio)tetrathiafulvalene (315 mg, 1.06 mmol) in dry THF (30 mL) at -78°C under N_2 atmosphere was added ^{n}BuLi (1.6 M in hexane, 0.728 mL, 1.16 mmol) and stirring continued for 1 h at -78°C. Tributylstannyl chloride (0.316 mL, 1.16 mmol) was added, the mixture was stirred for a further 1 h at -78°C. The temperature was allowed to rise to room temperature over a period of 2 h, and the solvent was evaporated, water was added (50 mL) and the mixture was extracted with dichloromethane (3×30 mL). The combined organic extracts were washed with water (3×30 mL), dried ($NaSO_4$), and the solvent was evaporated. Subsequently, dry toluene (20 mL) was added and N_2 gas bubbling was done for 20 min. After the bubbling, 2-(5-bromopyridin-2-yl)-1,3-benzothiazole (248 mg, 0.851 mmol) and $Pd(PPh_3)_2Cl_2$ (59.7 mg,

0.0851 mmol) were added and the mixture was heated overnight at 120°C. The solvent was evaporated. The resulting residue was purified by a column-chromatography on silica gel with CH_2Cl_2/*n*-hexane (2/1, v/v) as an eluent. Compound **L** was afforded as a purple solid (155 mg, 36%); m.p. 213-215°C (decomp.) Rf=0.45 (dichloromethane/hexane=2/1)

^{1}H NMR (400 MHz, $CDCl_3$): δ 8.73 (d, *J*=2.0 Hz, 1H, pyridine), 8.36 (d, *J*=8.4 Hz, 1H, BZT), 8.10 (d, *J*=8.4 Hz, 1H, BZT), 7.96 (d, *J*=8.0 Hz, 1H, pyridine), 7.81 (dd, *J*=8.0 Hz, *J*=2.0 Hz, 1H, pyridine), 7.52 (dd, J_1=8.0 Hz, J_2=7.2 Hz, 1H, BZT) 7.43 (dd, J_1=8.0 Hz, J_2=7.2 Hz, 1H, BZT), 6.76 (s, 1H, TTF), 2.46 (s, 3H, SMe), 2.45 (s, 3H, SMe)

HRMS (FAB+, Matrix=3-Nitrobenzyl alcohol) ($C_{20}H_{12}N_2S_7$): Found 505.9202; Calcd. 505.9198

IR (KBr) ν 757,982, 1569, 3049, 3446 cm^{-1}

Synthesis of complexes

[Ln(tta)$_3$(L)]·CH$_2$Cl$_2$ (Ln=Eu (Eu(t)) and Dy (Dy(t))). 0.02 mmol of Ln(tta)$_3$·2H$_2$O (17.0 mg for Ln=Eu and 17.2 mg for Ln=Dy) were dissolved in 10 mL of CH_2Cl_2 and then added to a solution of 10 mL of CH_2Cl_2 containing 10.4 mg of L (0.02 mmol). After 20 minutes of stirring, 30 mL of *n*-hexane were layered at room temperature in the dark. Slow diffusion following by slow evaporation leads to purple single crystals (prisms) which are suitable for X-ray studies. Yield 24.2 mg (86 %) and 8.2 mg (29 %) respectively for **Eu(t)** and **Dy(t)**. Anal. Calcd (%) for $C_{45}H_{28}Cl_2EuF_9N_2O_6S_{10}$: C 38.38, H 1.99, N 1.99; found: C 38.59, H 2.06 N, 2.11. Anal. Calcd (%) for $C_{45}H_{28}Cl_2DyF_9N_2O_6S_{10}$: C 38.09, H 1.98, N 1.98; found: C 38.22, H 2.01 N, 2.07.

[Ln(tta)$_3$(L)] (Ln=Dy (Dy(m)) and Y (Y(m)). 0.02 mmol of Ln(tta)$_3$·2H$_2$O (17.2 mg for Ln=Dy, 15.8 mg for Ln=Y, 17.3 mg for Ln=Er and 17.5 mg for Ln=Yb) were dissolved in 10 mL of CH_2Cl_2 and then added to a solution of 10 mL of CH_2Cl_2 containing 10.4 mg of L (0.02 mmol). After 20 minutes of stirring, 30 mL of *n*-hexane were layered at room temperature in the dark. Slow diffusion following by slow evaporation leads to purple single crystals (sticks) which are suitable for X-ray studies. Yield 17.1 mg (64 %) and 22.9 mg (91 %) respectively for **Dy(m)** and **Y(m)**. Anal. Calcd (%) for $C_{44}H_{26}F_9N_2O_6S_{10}Dy$: C 39.61, H 1.95, N 2.10; found: C 39.49, H 2.00 N, 2.05. Anal. Calcd (%) for $C_{44}H_{26}F_9N_2O_6S_{10}Y$: C 41.93, H 2.06, N 2.22; found: C 42.01, H 1.99 N, 2.11. Anal. Calcd (%) for $C_{44}H_{26}F_9N_2O_6S_{10}Er$: C 39.48, H 1.94, N 2.09; found: C 39.52, H 2.01 N, 2.13. Anal. Calcd (%) for $C_{44}H_{26}F_9N_2O_6S_{10}Yb$: C 39.31, H 1.94, N 2.08; found: C 38.99, H 1.67 N, 2.14.

[Dy$_{0.02}$Y$_{0.98}$(tta)$_3$(L)] (Dy$_{0.02}$Y$_{0.98}$(m)). 1.0 mg of Dy(tta)$_3$·2H$_2$O (0.0012 mmol) and 46.3 mg of Y(tta)$_3$·2H$_2$O (0.0588 mmol) were dissolved in 10 mL of CH_2Cl_2 and then added to a solution of 10 mL of CH_2Cl_2 containing 31.2 mg of L (0.06 mmol). After 20 minutes of stirring, 30 mL of *n*-hexane were layered at room temperature in the dark. Slow diffusion following by slow evaporation leads to purple single crystals (sticks) which are suitable for X-ray studies. Yield 67.3 mg (89 %). Anal. Calcd (%) for $C_{44}H_{26}F_9N_2O_6S_{10}Dy_{0.02}Y_{0.98}$: C 41.60, H 2.05, N 2.21; found: C 41.59, H 2.00 N, 2.15.

[^{164}Dy$_{0.07}$Y$_{0.93}$(tta)$_3$(L)] (^{164}Dy$_{0.07}$Y$_{0.93}$(m)). This compound was prepared from the experimental protocol of (**Dy$_{0.02}$Y$_{0.98}$(m)**) starting from 2.6 mg ^{164}Dy(tta)$_3$·2H$_2$O instead of 1 mg of Dy(tta)$_3$·2H$_2$O. Yield 63.7 mg (84 %). Anal. Calcd (%) for $C_{44}H_{26}F_9N_2O_6S_{10}Dy_{0.07}Y_{0.93}$: C 41.80, H 2.06, N 2.22; found: C 41.79, H 2.03 N, 2.25.

[^{164}Dy$_{0.05}$Eu$_{0.95}$(tta)$_3$(L)] (^{164}Dy$_{0.05}$Eu$_{0.95}$(t)). 2.6 mg of ^{164}Dy(tta)$_3$·2H$_2$O (0.003 mmol) and 48.5 mg of Eu(tta)$_3$·2H$_2$O (0.057 mmol) were dissolved in 10 mL of CH_2Cl_2 and then added to a solution of 10 mL of CH_2Cl_2 containing 31.2 mg of L (0.06 mmol). After 20 minutes of stirring, 30 mL of *n*-hexane were layered at room temperature in the dark. Slow diffusion following by slow evaporation leads to purple single crystals (prisms) which are suitable for X-ray studies. Yield 65.0 mg (77 %). Anal. Calcd (%) for $C_{45}H_{28}Cl_2F_9N_2O_6S_{10}Dy_{0.05}Eu_{0.95}$: C 38.39, H 1.99, N 1.99; found: C 38.44, H 2.00 N, 2.04.

Crystallography. Single crystals of **Eu(t)**, **Dy(t)**, **Dy(m)** and **Y(m)** were mounted on a APEXII Bruker-AXS diffractometer (MoK_α radiation source, λ=0.71073 Å, T=150(2) K) for data collection, from the Centre de Diffractométrie (CDIFX), Université de Rennes 1, France. Structures were solved with a direct method using the SIR-97 program and refined with a full matrix least-squares method on F^2 using the SHELXL-97 program[5] for all the compounds. The cell and X-ray powder diffraction are performed for **$^{164}Dy_{0.07}Y_{0.93}$(m)** and **$^{164}Dy_{0.05}Eu_{0.95}$(t)**. The wide angle X-ray diffraction pattern of the sample was recorded on a Bruker AXS diffractometer with mono-chromatized CuKα radiation (λ=1.5406 Å), operating at 40 kV, 40 mA, with 0.0079° step size and a counting time of 358 ms per step, over a range of $3° < 2\theta < 80°$, at room temperature. Crystallographic data are summarized in end notes. Complete crystal structure results as a CIF file including bond lengths, angles, and atomic coordinates are deposited as Supporting Information. CCDC numbers 1510233, 1510234, 1510236 and 1510237 are for **Eu(t)**, **Dy(t)**, **Dy(m)** and **Y(m)**, respectively.

Physical Measurements. The elementary analyses of the compounds were performed at the Centre Régional de Mesures Physiques de l'Ouest, Rennes. ^{1}H NMR was recorded on a Bruker Ascend 400 spectrometer. Chemical shifts are reported in parts per million referenced to TMS for ^{1}H NMR. Cyclic voltametry was carried out in CH_2Cl_2 solution, containing 0.1 M $N(C_4H_9)_4PF_6$ as supporting electrolyte. Voltamograms were recorded at 100 mV s^{-1} at a platinum disk electrode. The potentials were measured *versus* a saturated calomel electrode (SCE). The dc magnetic susceptibility measurements were performed on solid polycrystalline sample with a Quantum Design MPMS-XL SQUID magnetometer between 2 and 300 K in an applied magnetic field of 200 Oe in the 2-20 K temperature range, 2 kOe between 20 and 80 K and 10 kOe between 80 and 300 K. These measurements were all corrected for the diamagnetic contribution as calculated with Pascal's constants.

Computational Details. Wavefunction-based calculations were carried out on **Dy(t)** and **Dy(m)** by using the SA-CASSCF/RASSI-SO approach, as implemented in the MOLCAS quantum chemistry package (versions 8.0).[6] In this approach, the relativistic effects are treated in two steps on the basis of the Douglas–Kroll Hamiltonian. First, the scalar terms were included in the basis-set generation and were used to determine the spin-free wavefunctions and energies in the complete active space self-consistent field (CASSCF) method.[7] Next, spin-orbit coupling was added within the restricted-active-space-state-interaction (RASSI-SO) method, which uses the spin-free wavefunctions as basis states.[8,9] The resulting wavefunctions and energies are used to compute the magnetic properties and g-tensors of the lowest states from the energy spectrum by using the pseudo-spin S=1/2 formalism in the SINGLE-ANISO routine.[10] Cholesky decomposition of the bielectronic integrals was employed to save disk space and speed-up the calculations.[11] The atomic positions were extracted from the X-ray crystal structures. Only the H and F atom positions were optimized using the DFT procedure described previously. The active space of the self-consistent field (CASSCF) method consisted of the nine 4f electrons of the Dy^{III} ion spanning the seven 4f orbitals, i.e. CAS(9,7)SCF. State-averaged CASSCF calculations were performed for all of the sextets (21 roots), all of the quadruplets (224 roots), and 300 out of the 490 doublets (due to software limitations) of the Dy^{III} ion. Twenty-one sextets, 128 quadruplets, and 107 doublets were mixed through spin−orbit coupling in RASSI-SO. All atoms were described by ANO-RCC basis sets.[12-14] The following contractions were used: [8s7p4d3f2g1h] for Dy, [4s3p2d] for the O and N atoms directly coordinated to Dy, [4s3p] for the S atoms, [3s2p] for the C and F atoms and [2s] for the H atoms.

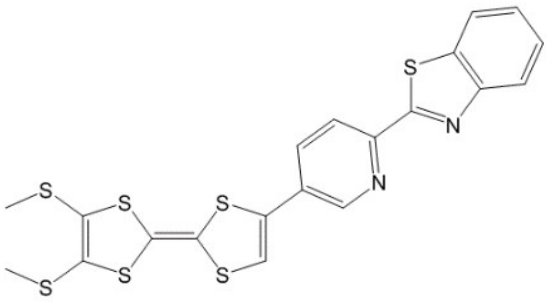

(L)

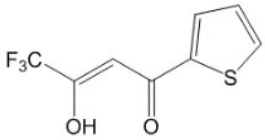

Htta

Scheme S1. Molecular structure of **L** and Htta$^-$.

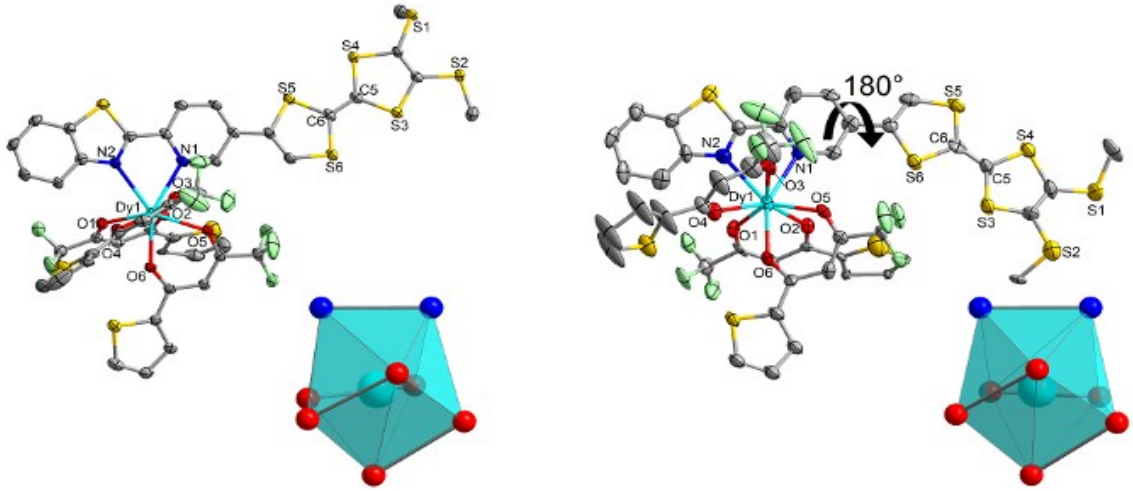

Figure S1. Representation of the complex [Dy(tta)$_3$**L**] in **Dy(t)** (left) and **Dy(m)** (right) with the coordination polyhedra in both structures (cyan, Dy; green, F; yellow, S; gray, C; blue, N; red, O). Thick lines on edges of polyhedra feature the atoms coming from the same bidentate ligand. ORTEP views of the asymmetric unit show thermal ellipsoids drawing at 30% probability. Hydrogen atoms and CH_2Cl_2 molecule of crystallisation are omitted for clarity.

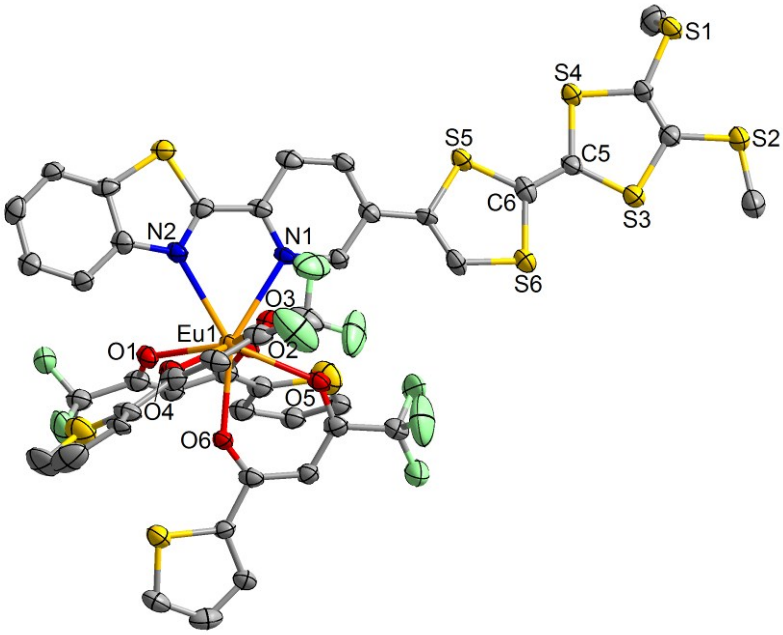

Figure S2. ORTEP view of the asymmetric unit for **Eu(t)**. Thermal ellipsoids are drawn at 30% probability. Hydrogen atoms and CH_2Cl_2 molecule of crystallisation are omitted for clarity.

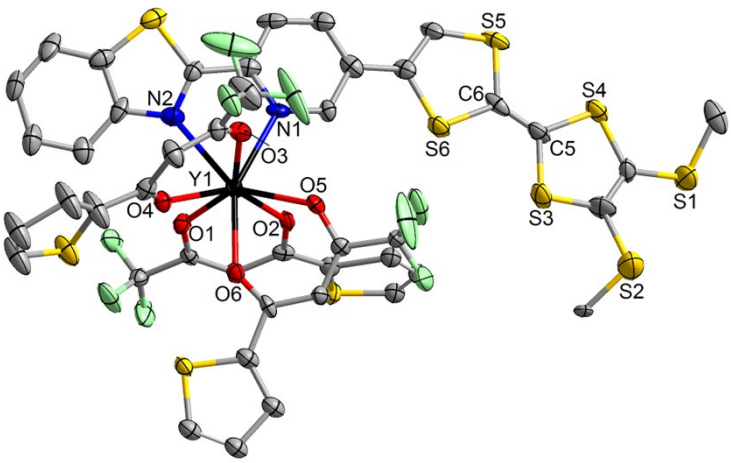

Figure S3. ORTEP view of the asymmetric unit for **Y(m)**. Thermal ellipsoids are drawn at 30% probability. Hydrogen atoms are omitted for clarity.

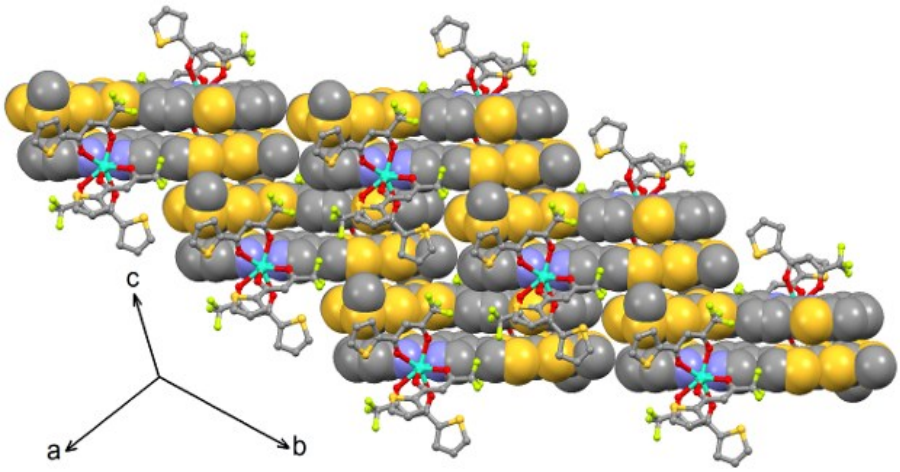

Figure S4. Crystal packing of **Dy(t)**. Hydrogen atoms and CH_2Cl_2 molecule of crystallisation are omitted for clarity. Donor-Donor (D-D) interactions between the TTF cores (S2···S6=3.860 Å and S3···S6=3.856 Å), Acceptor-Acceptor (A-A) interactions between the benzothiazole-2-pyridine moieties (S7···S7=3.820 Å), D-A interactions through π-π stacking and finally short S···S contacts are identified between the TTF core and the thiophene ring of the tta^- anion (S2···S8=3.488 Å).

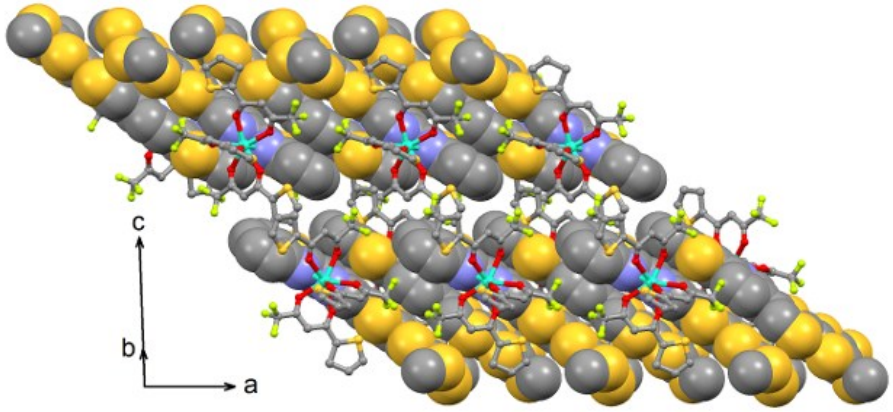

Figure S5. Crystal packing of **Dy(m)**. Hydrogen atoms are omitted for clarity. The crystal packing of **Dy(m)** is sensibly different compared to the one of **Dy(t)** due to the rotation of **L** (Fig. S5). The ligands are now packed along the *a* axis through the S2···S5=3.731 Å contacts while the 1D organic networks interact through S···S contacts between the thiomethyl groups and the thiophene rings of tta^- anions (S1···S10=3.730 Å and S2···S10=3.746 Å).

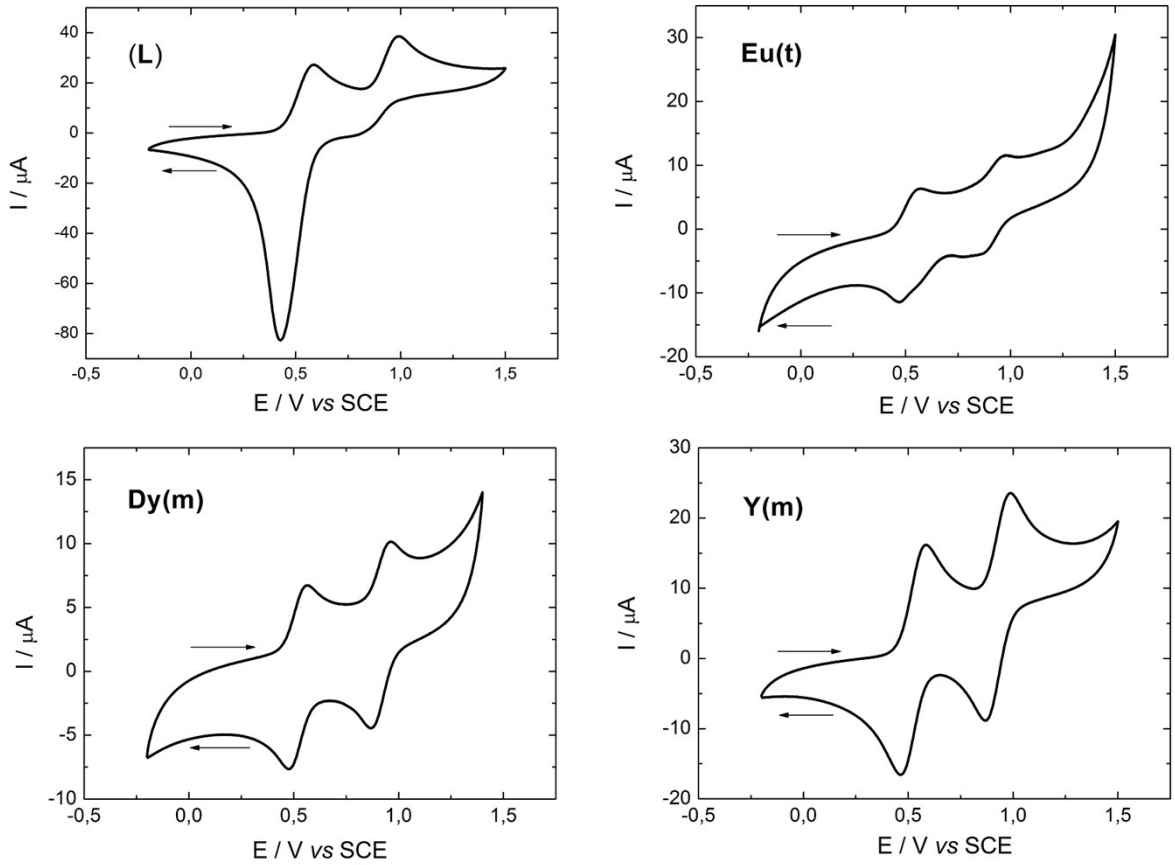

Figure S6. Cyclic voltammograms of the ligand **L** and representative complexes in CH_2Cl_2 at a scan rate of 100 mV.s^{-1}. The potentials were measured versus a saturated calomel electrode (SCE); Pt wire as the counter electrodes.

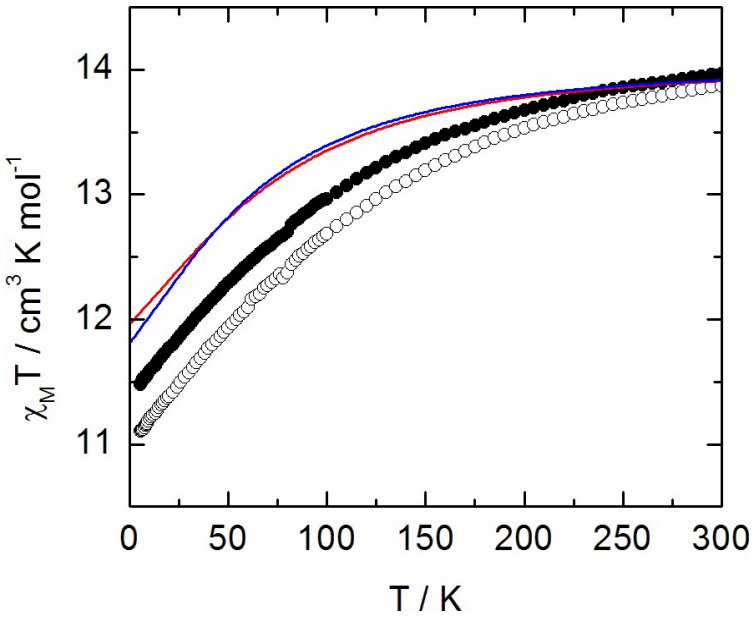

Figure S7. Temperature dependences of $\chi_M T$ for pelletized samples of **Dy(t)** (full symbols) and **Dy(m)** (empty symbols) with the calculated curves in red and blue for **Dy(t)** and **Dy(m)**, respectively.

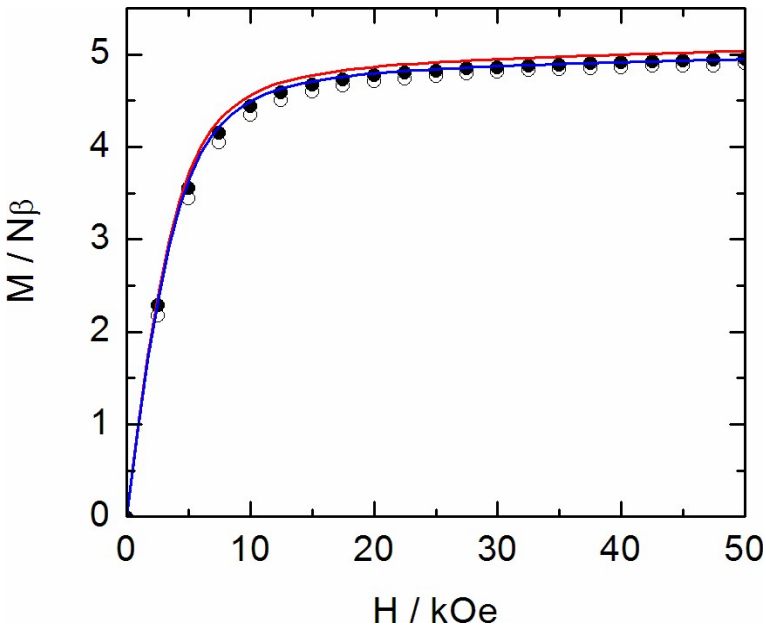

Figure S8. Magnetic field dependences of the magnetization at 2 K for pelletized samples of **Dy(t)** (full symbols) and **Dy(m)** (empty symbols) with the calculated curves in red and blue for **Dy(t)** and **Dy(m)**, respectively.

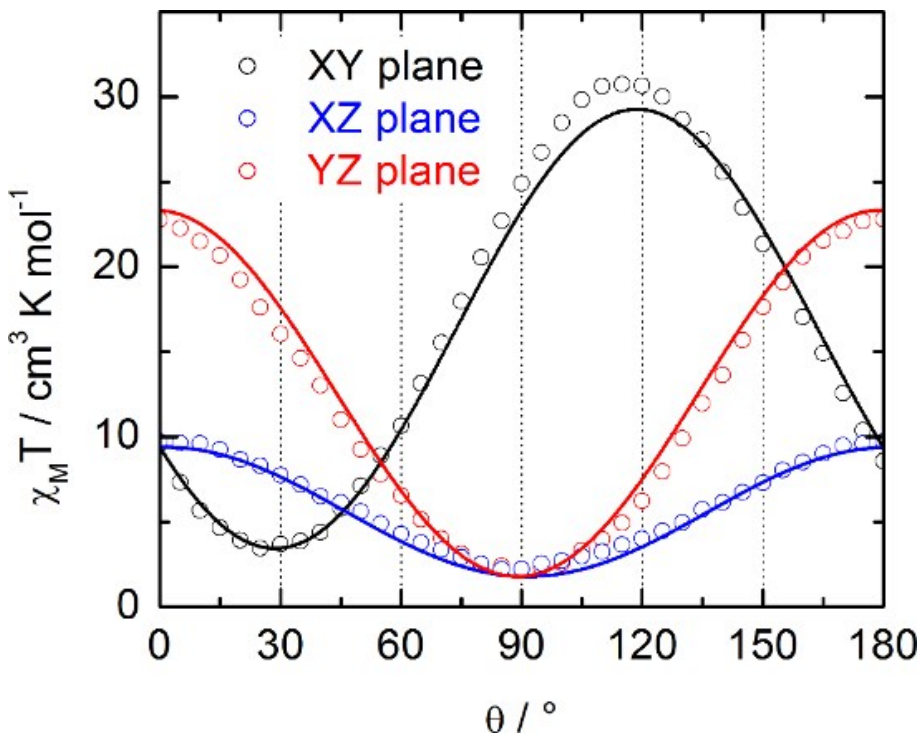

Figure S9. Angular dependence of $\chi_M T$ of oriented single crystals of **Dy(t)** rotating in three perpendicular planes with H=1 kOe at 2 K (see ESI for plane definitions). Best fitted curves in full lines.

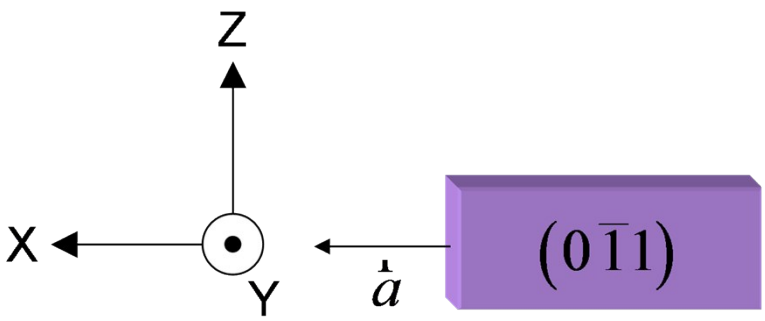

Figure S10. Oriented single crystal of **Dy(t)** with the XYZ crystal reference frame.

Susceptibility tensor in the crystal frame (XYZ):

$$\chi_M T = \begin{pmatrix} 9.388 & -10.87 & 0.186 \\ -10.87 & 23.32 & -0.396 \\ 0.186 & -0.396 & 1.793 \end{pmatrix} \text{cm}^3\ \text{K mol}^{-1}$$

Principal values and direction of the susceptibility tensor in the XYZ crystal frame:

$$\chi_{xx}T\begin{pmatrix}0.877\\0.480\\-0.016\end{pmatrix}=3.44,\ \chi_{yy}T\begin{pmatrix}0.480\\-0.877\\0.016\end{pmatrix}=29.27,\ \chi_{zz}T\begin{pmatrix}-0.007\\-0.022\\-0.999\end{pmatrix}=1.79\ \text{cm}^3\ \text{K mol}^{-1}$$

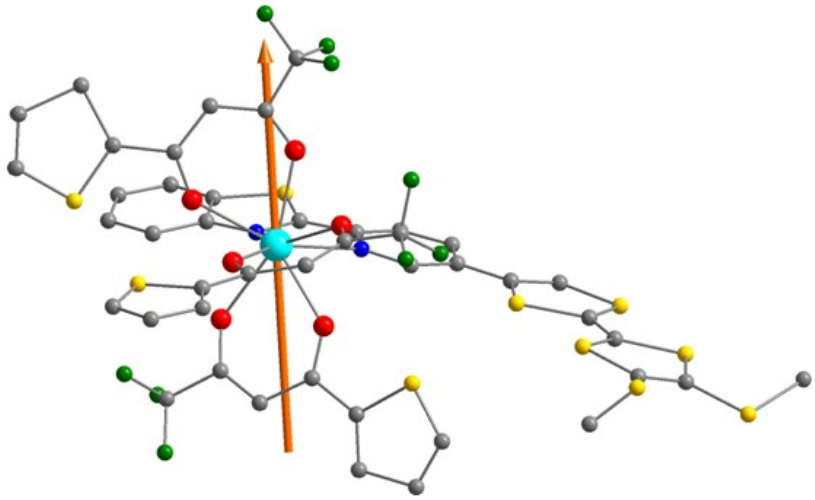

Figure S11. Representation of the crystallographic structure of [Dy(tta)$_3$**L**] in **Dy(m)** with the theoretical magnetic anisotropy axis in orange. H atoms and solvent molecule have been omitted for clarity in both representations.

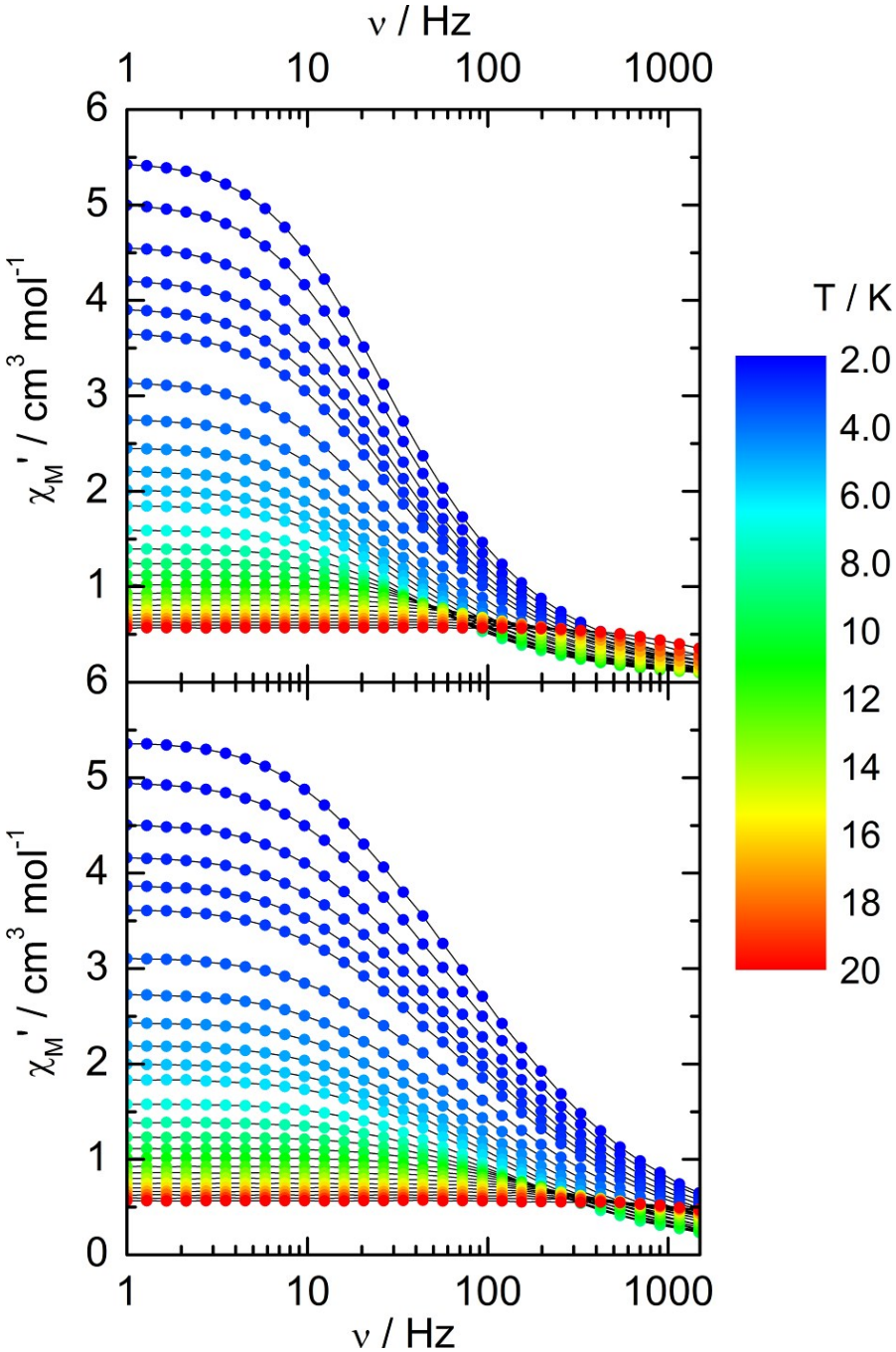

Figure S12. (top) Frequency dependence of the in-phase component, χ_M', of the ac susceptibility between 2 and 20 K for **Dy(t).** (bottom) Frequency dependence of the in-phase component, χ_M', of the ac susceptibility between 2 and 20 K for **Dy(m)**.

Extended Debye model.

$$\chi' = \chi_S + (\chi_T - \chi_S)\frac{1+(\omega\tau)^{1-\alpha}\sin\left(\alpha\frac{\pi}{2}\right)}{1+2(\omega\tau)^{1-\alpha}\sin\left(\alpha\frac{\pi}{2}\right)+(\omega\tau)^{2-2\alpha}}$$

$$\chi'' = (\chi_T - \chi_S)\frac{(\omega\tau)^{1-\alpha}\cos\left(\alpha\frac{\pi}{2}\right)}{1+2(\omega\tau)^{1-\alpha}\sin\left(\alpha\frac{\pi}{2}\right)+(\omega\tau)^{2-2\alpha}}$$

With χ_T the isothermal susceptibility, χ_S the adiabatic susceptibility, τ the relaxation time and α the empiric parameter which describes the distribution of the relaxation time. For SMM with only one relaxing object α is close to zero. The extended Debye model was applied to fit simultaneously the experimental variations of χ' and χ'' with the frequency f of the oscillating field ($\omega = 2\pi\nu$). Typically, only the temperatures for which a maximum on the χ'' vs. ν curves have been considered (see figure here below for an example). The best fitted parameters τ, α, χ_T, χ_S are listed in Tables S6 and S7 with the coefficient of determination R^2.

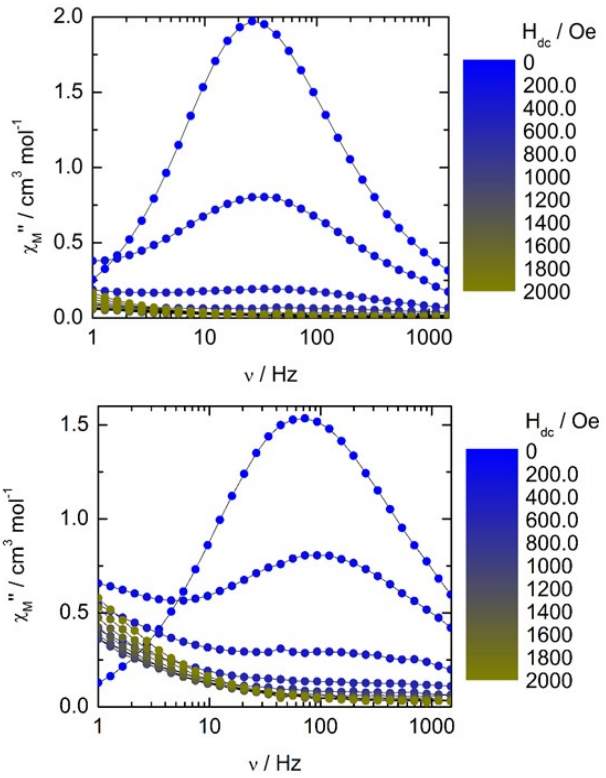

Figure S13. (top) Frequency dependence of the out-of-phase component, χ_M'', of the ac susceptibility at 2 K for **Dy(t)** (top) and **Dy(m)** (bottom) as a function of the external field.

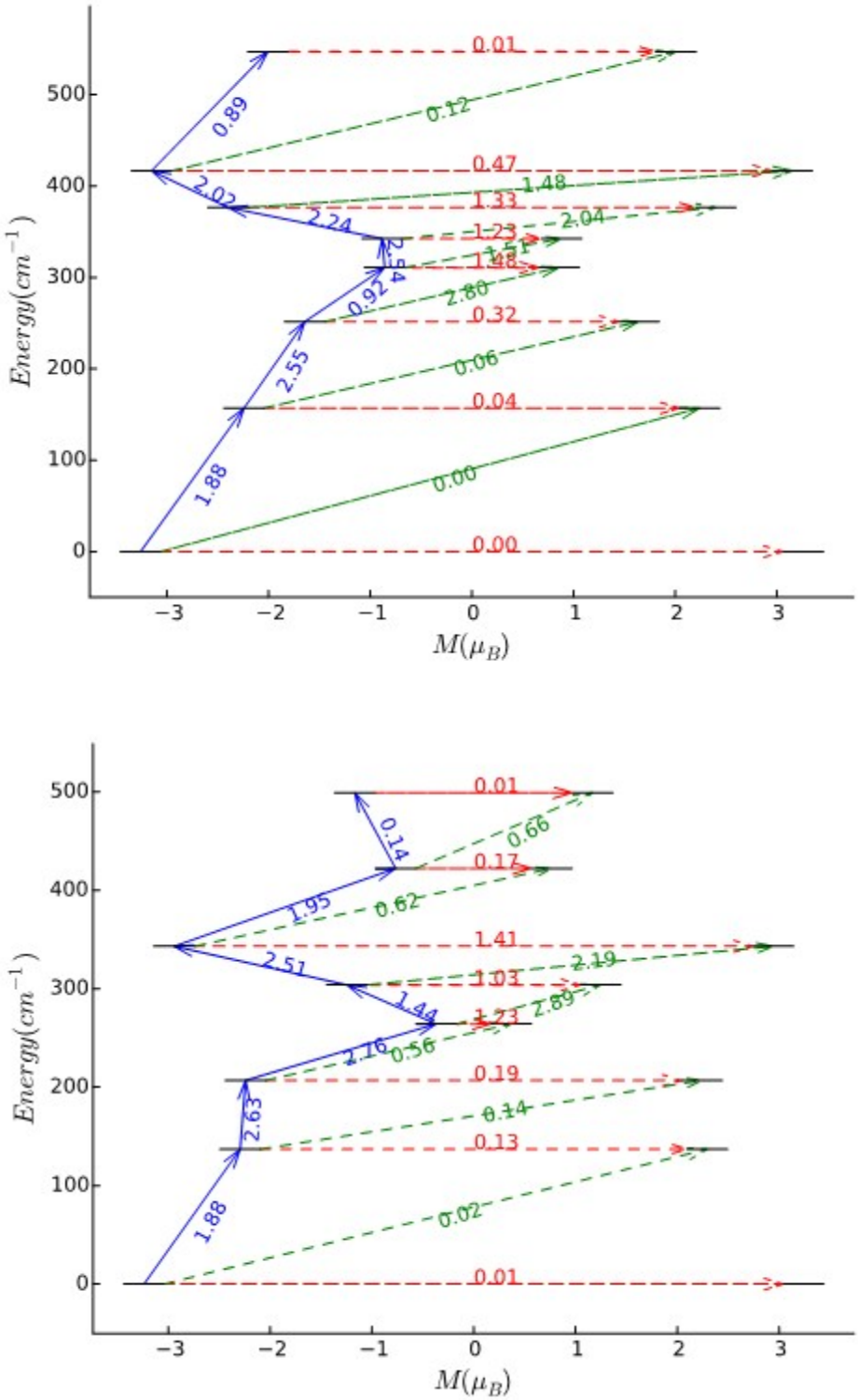

Figure S14. Magnetization blocking barrier of **Dy(t)** (top) and **Dy(m)** (bottom). The black lines represent components of the ground-state multiplet, while the arrows connecting them represent the relaxation paths. The number at each path is the average transition dipole moment.

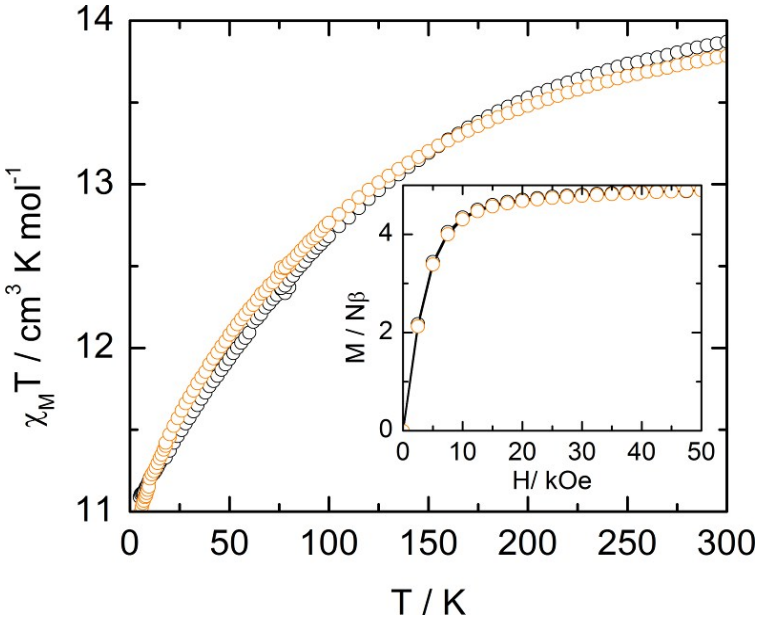

Figure S15. Temperatures dependences of $\chi_M T$ for pelletized samples of **Dy(m)** (black) and **^{164}Dy(m)** (orange). Inset: Magnetic field dependences of the magnetization at 2 K for pelletized samples of **Dy(m)** (black) and **^{164}Dy(m)** (orange).

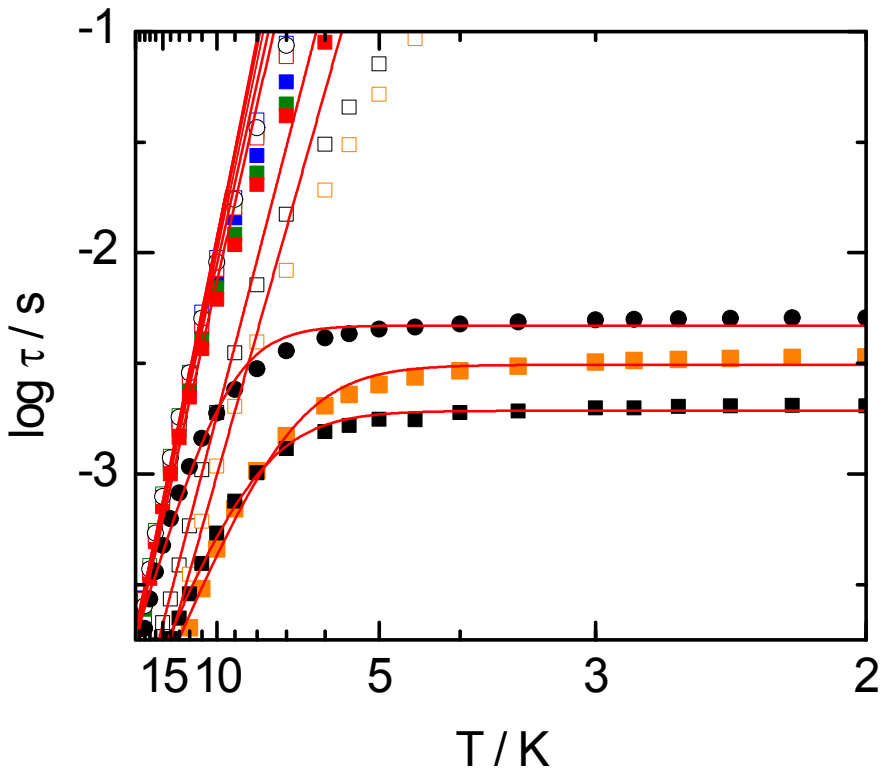

Figure S16. Log scale plots of the temperature dependence of the relaxation of the magnetic moment in **Dy(m)** (black squares), **Dy(t)** (black circles), **^{164}Dy(m)** (orange), **$Dy_{0.02}Y_{0.98}$(m)** (blue), **$^{164}Dy_{0.07}Y_{0.93}$(m)** (olive) and **$^{164}Dy_{0.05}Eu_{0.95}$(t)** (red) at zero external field (full symbols) and at 1 kOe (empty symbols). Red lines correspond to the best-fitted curves with Arrhenius or modified Arrhenius laws (see text).

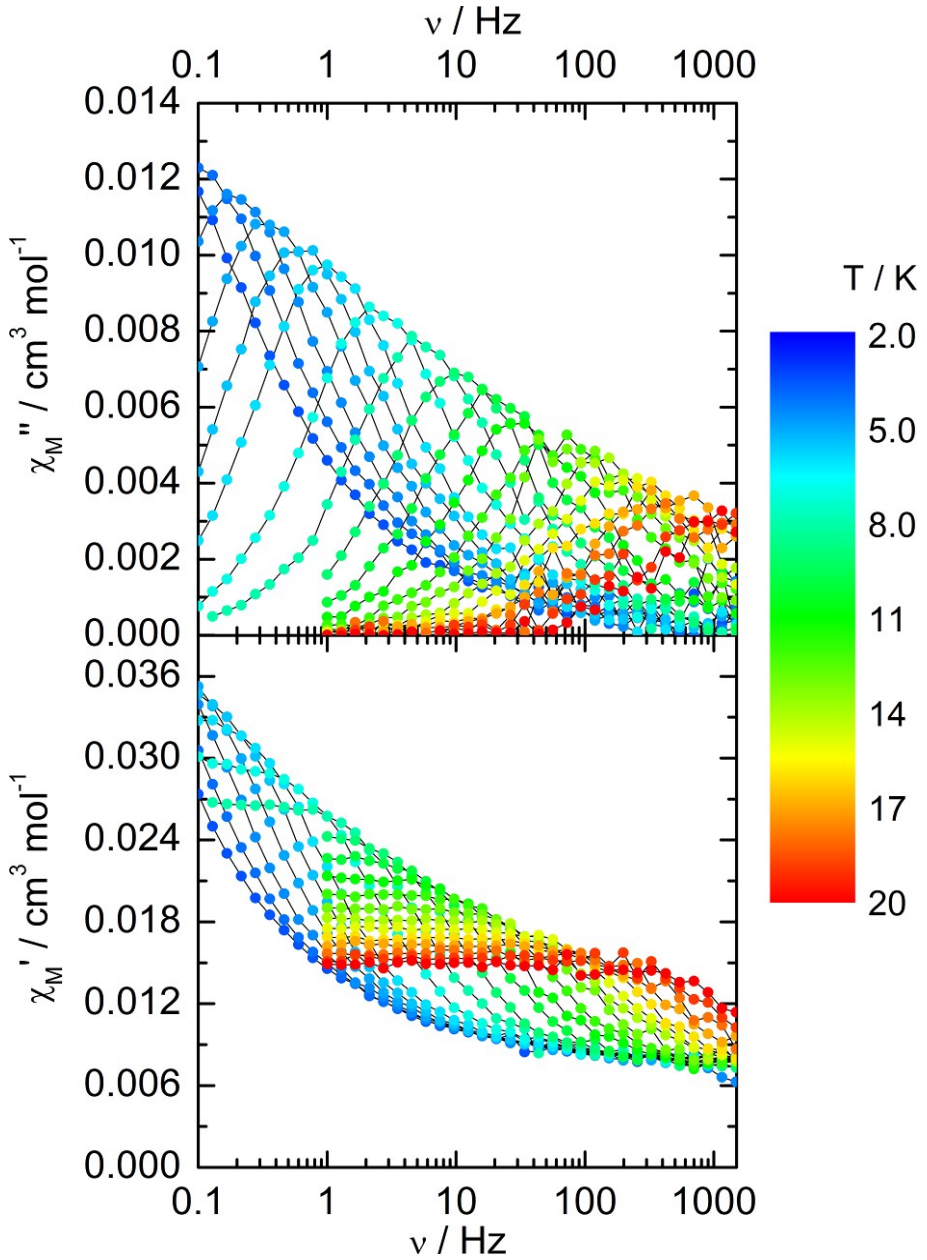

Figure S17. Frequency dependences of the in-phase, χ_M' (bottom), and out-of-phase, χ_M'' (top), components of the ac susceptibility between 3.5 and 18 K for **$Dy_{0.02}Y_{0.98}$(m)** measured at zero external dc field.

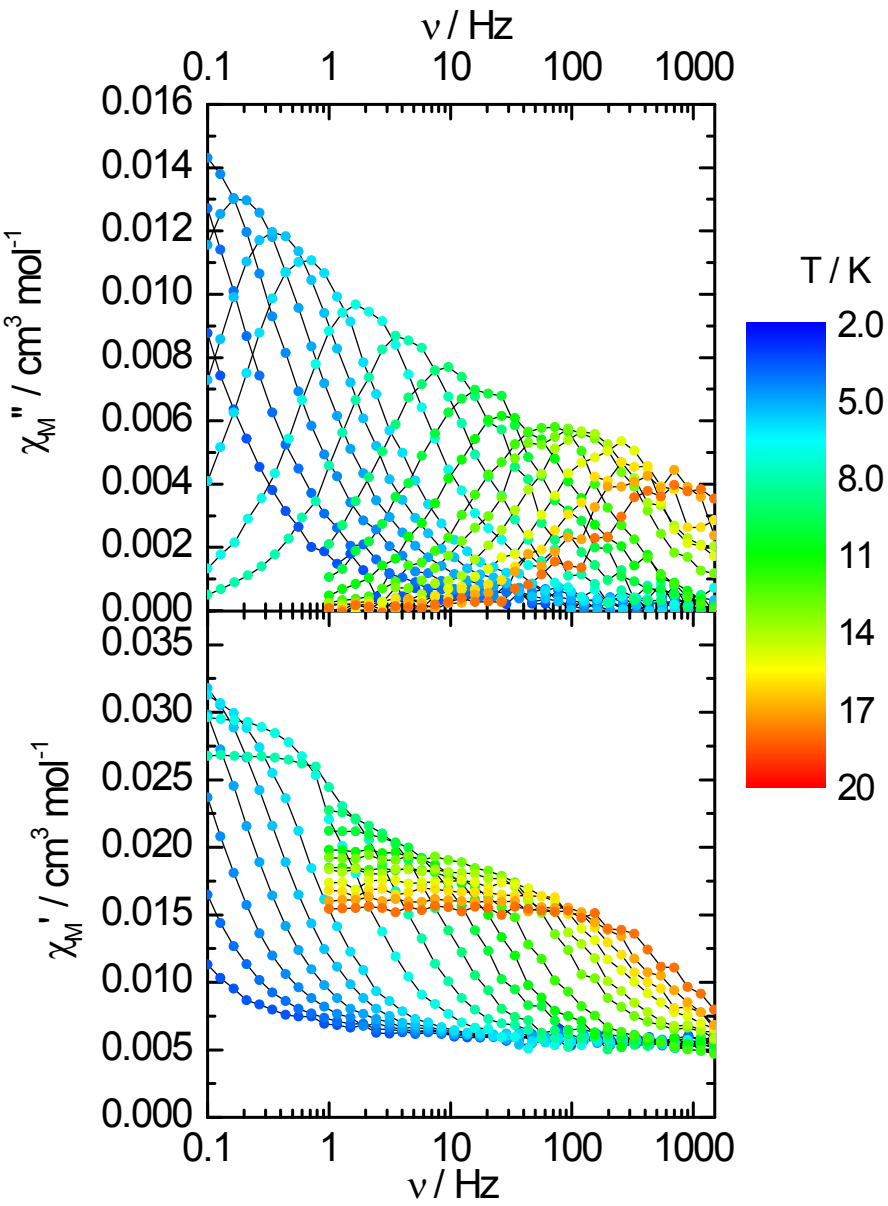

Figure S18. Frequency dependences of the in-phase, χ_M' (bottom), and out-of-phase, χ_M'' (top), components of the ac susceptibility between 3.5 and 18 K for **$Dy_{0.02}Y_{0.98}$(m)** measured at 1 kOe.

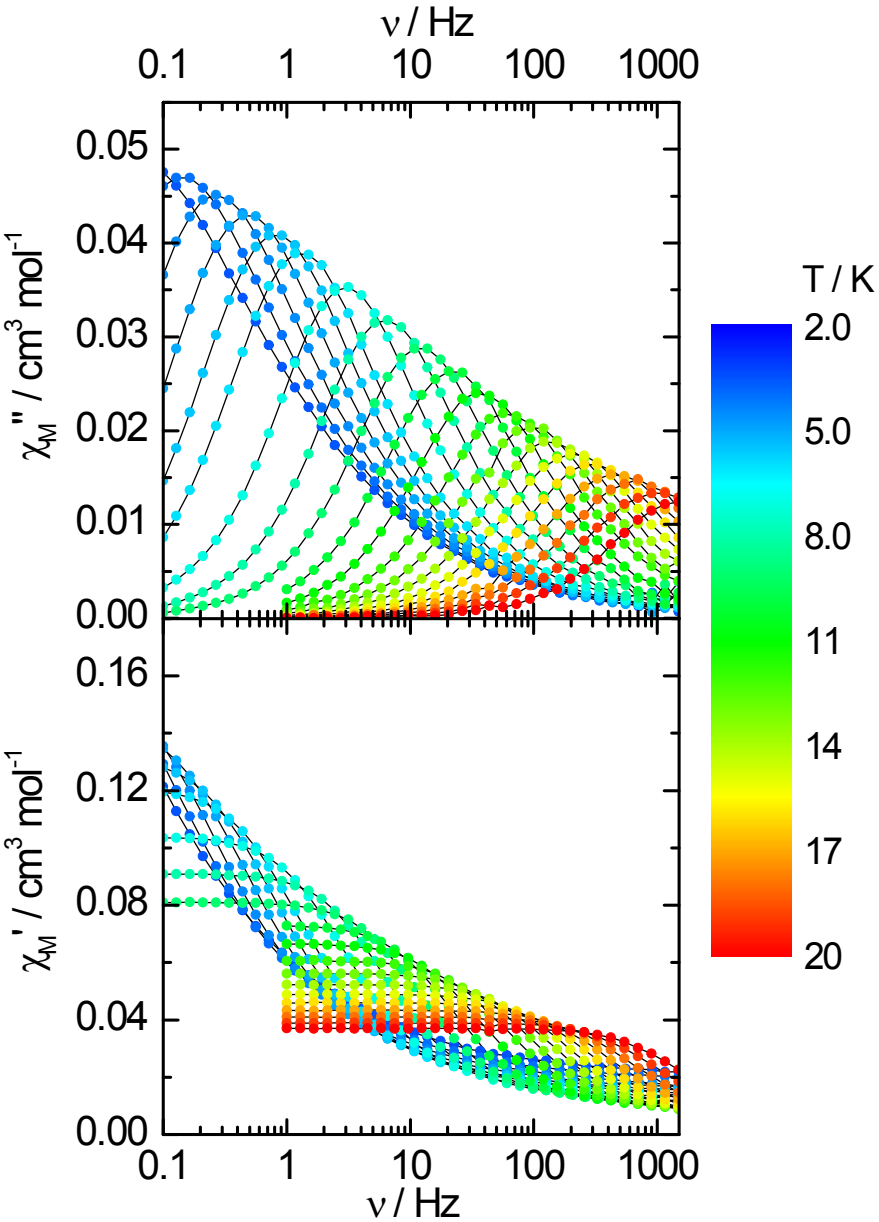

Figure S19. Frequency dependences of the in-phase, χ_M' (bottom), and out-of-phase, χ_M'' (top), components of the ac susceptibility between 3.5 and 20 K for **$^{164}Dy_{0.07}Y_{0.93}$(m)** measured at zero external dc field.

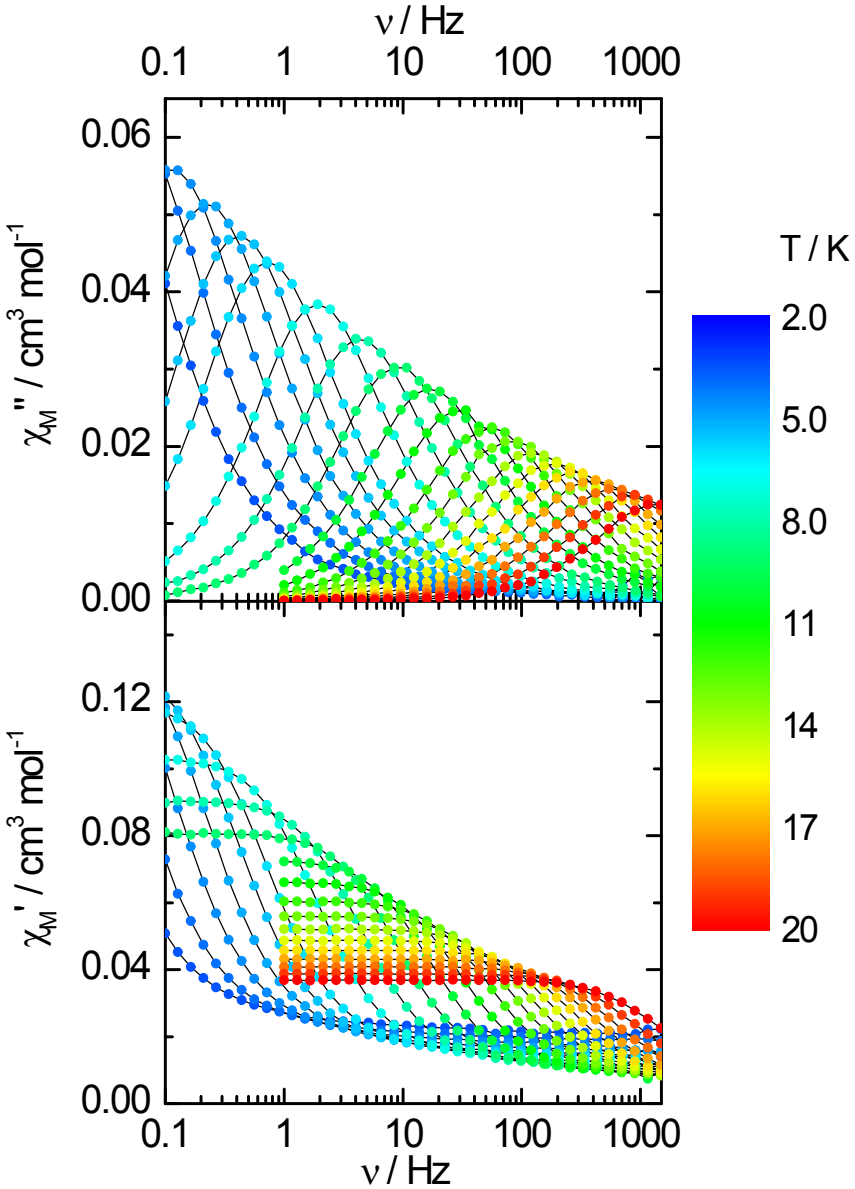

Figure S20. Frequency dependences of the in-phase, χ_M' (bottom), and out-of-phase, χ_M'' (top), components of the ac susceptibility between 3.5 and 20 K for **$^{164}Dy_{0.07}Y_{0.93}$(m)** measured at 1 kOe.

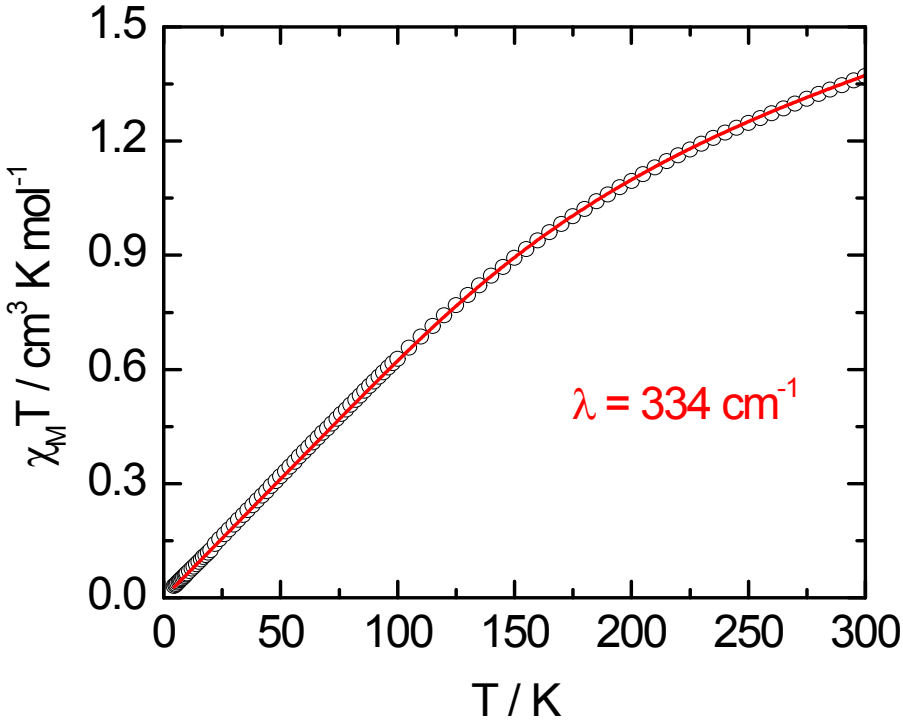

Figure S21. Temperature variation of $\chi_M T$ for **Eu(t)** with the best-fitted curve (see here below).

<u>Magnetism of Eu^{III} complexes:</u>

The spin-orbit coupling operator is:

$\hat{H} = \lambda \hat{\boldsymbol{L}} \cdot \hat{\boldsymbol{S}}$ where λ is the spin-orbit coupling parameter.

The energies of $\boldsymbol{J} = \boldsymbol{L} + \boldsymbol{S}$ states are:

$E(J) = \lambda J(J+1)/2$ where the energy of $^7F_0$ state has been taken as the origin.

The magnetic susceptibility considering that excited states (^7F_J with $J = 1$ to 5) can be thermally populated is expressed as

$$\chi_M = \frac{\sum_{J=0}^{6}(2J+1)\chi_M(J)\exp\left[\frac{-\lambda J(J+1)}{2kT}\right]}{\sum_{J=0}^{6}(2J+1)\exp\left[\frac{-\lambda J(J+1)}{2kT}\right]}$$

With $\chi_M(J) = \frac{Ng_J^2\beta^2 J(J+1)}{3kT} + \frac{2N\beta^2(g_J-1)(g_J-2)}{3\lambda}$

g_J has its common meaning. The first term is the Curie law and the second term is the temperature Independent Paramagnetism (TIP) which is due to the field induced mixing with close excited states. In this frame χ_M can be rewritten:

$$\chi_M = \frac{N\beta^2}{3kTx} \frac{\left[\begin{array}{l} 24 + \left(\frac{27x}{2} - \frac{3}{2}\right)e^{-x} + \left(\frac{135x}{2} - \frac{5}{2}\right)e^{-3x} \\ + \left(189x - \frac{7}{2}\right)e^{-6x} + \left(405x - \frac{9}{2}\right)e^{-10x} \\ + \left(\frac{1485x}{2} - \frac{11}{2}\right)e^{-15x} + \left(\frac{2457x}{2} - \frac{13}{2}\right)e^{-21x} \end{array}\right]}{1 + 3e^{-x} + 5e^{-3x} + 7e^{-6x} + 9e^{-10x} + 11e^{-15x} + 13e^{-21x}}$$

With $x = \frac{\lambda}{kT}$

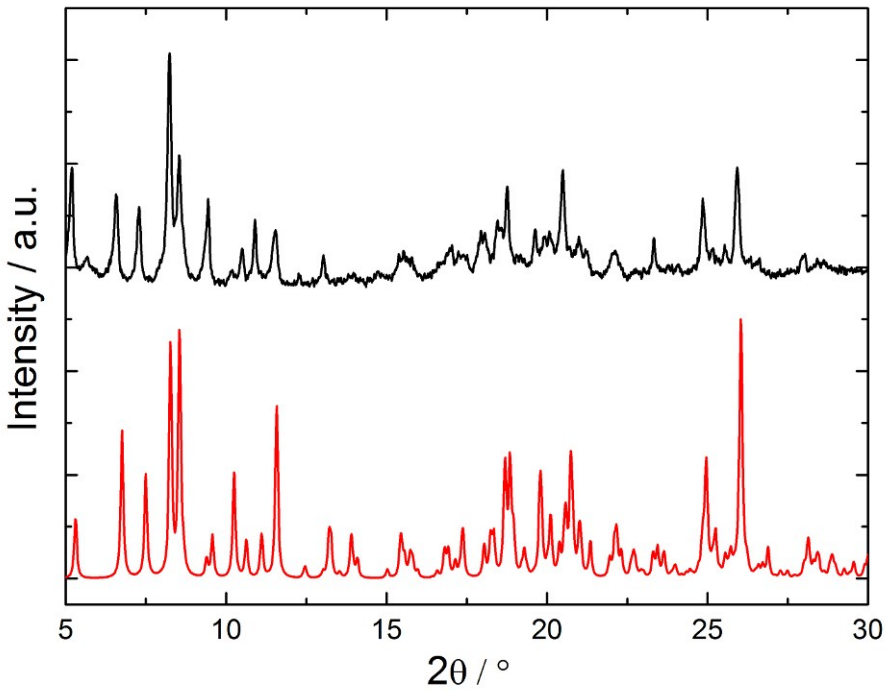

Figure S22. Superposition of experimental X-ray powder diffraction patterns from **^{164}Dy$_{0.05}$Eu$_{0.95}$(t)** (black) measured at 300 K and simulated from **Eu(t)** single-crystal data obtained at 150 K (red).

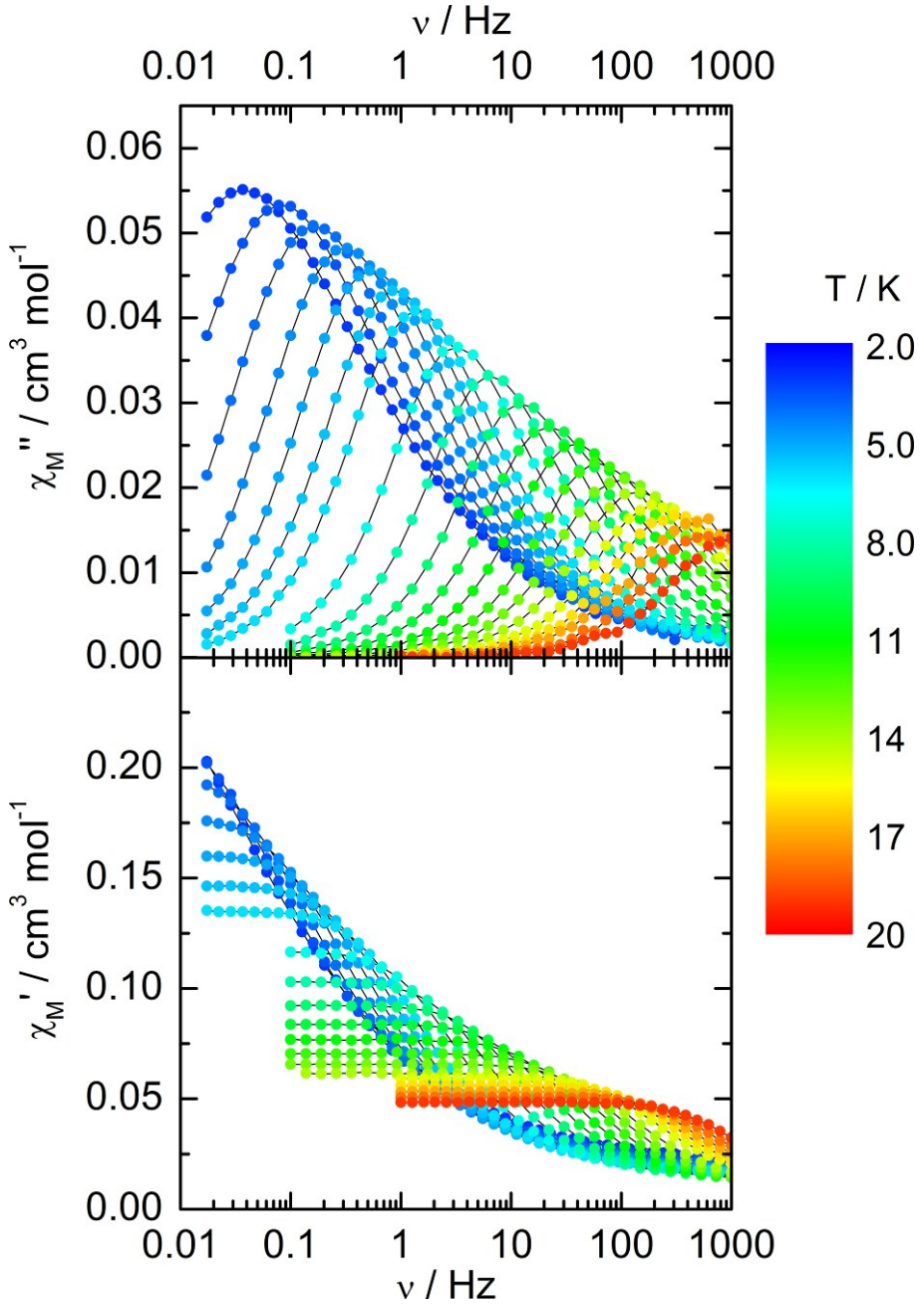

Figure S23. Frequency dependences of the in-phase, χ_M' (bottom), and out-of-phase, χ_M'' (top), components of the ac susceptibility between 3 and 19 K for **$^{164}Dy_{0.05}Eu_{0.95}$(t)** measured at zero external dc field.

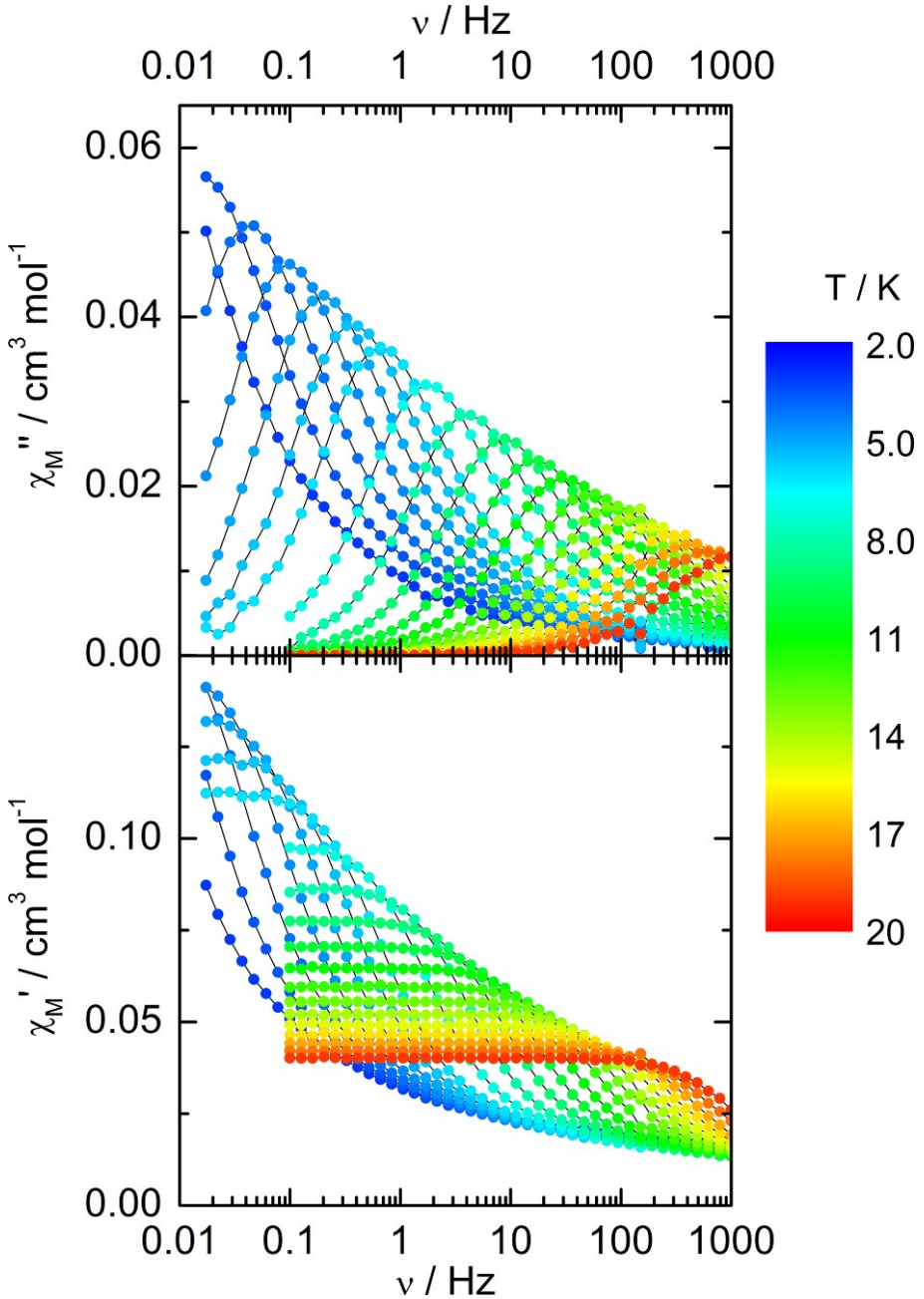

Figure S24. Frequency dependences of the in-phase, χ_M' (bottom), and out-of-phase, χ_M'' (top), components of the ac susceptibility between 3 and 19 K for **$^{164}Dy_{0.05}Eu_{0.95}$(t)** measured at 1 kOe.

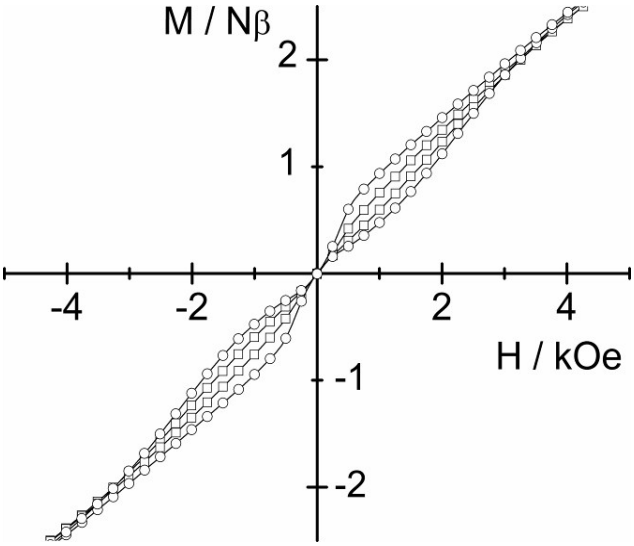

Figure S25. Magnetic hysteresis curves for **Dy(t)** (white circles) and **Dy(m)** (white squares) recorded at 3 K at a sweep rate of 16 Oe s^{-1}.

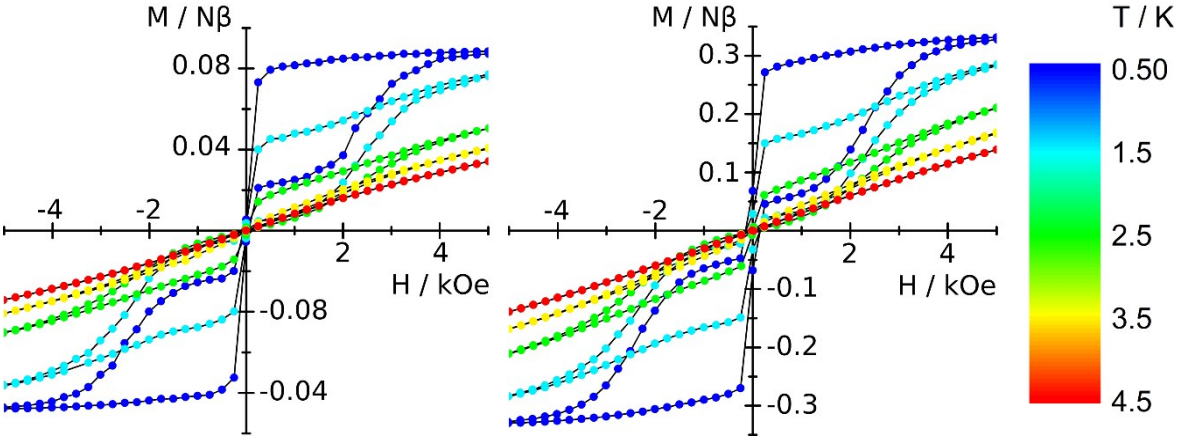

Figure S26. Hysteresis loops for **$Dy_{0.02}Y_{0.98}$(m)** (left) and **$^{164}Dy_{0.07}Y_{0.93}$(m)** (right) at various temperatures between 500 mK and 4.5 K at a sweep rate of 16 Oe s^{-1} (lines are eye guides only).

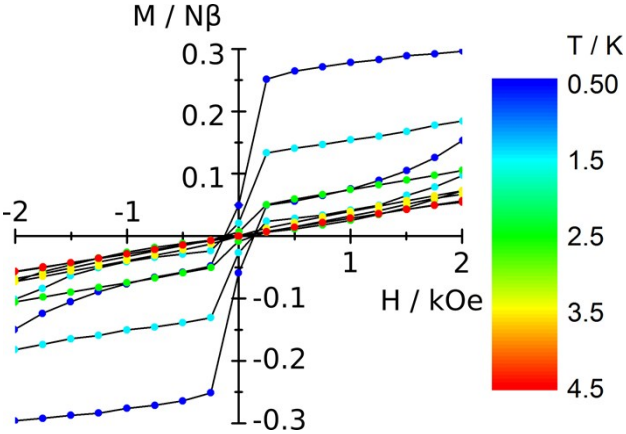

Figure S27. Hysteresis loops for **$^{164}Dy_{0.05}Eu_{0.95}$(t)** at various temperatures between 500 mK and 4.5 K at a sweep rate of 16 Oe s^{-1} (lines are eye guides only).

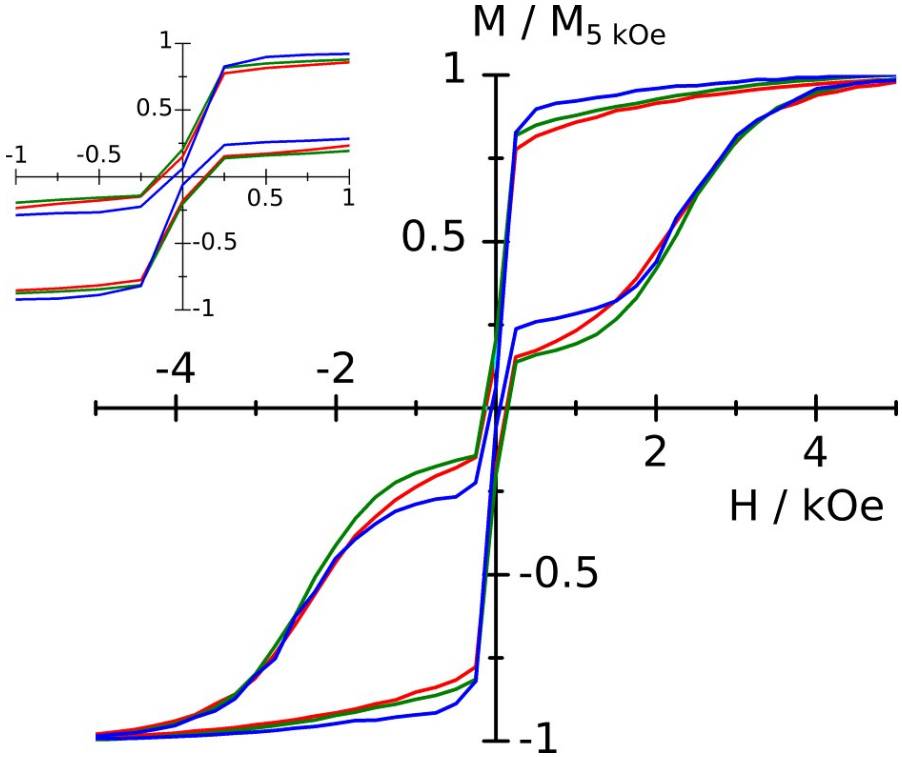

Figure S28. Hysteresis loops for **$^{164}Dy_{0.05}Eu_{0.95}$(t)** (red), **$Dy_{0.02}Y_{0.98}$(m)** (blue) and **$^{164}Dy_{0.07}Y_{0.93}$(m)** (olive) at 500 mK and at a sweep rate of 16 Oe s^{-1}. The inset is a zoom on the origin.

Table S1. X-ray crystallographic data for the complexes.

Compounds	$[Eu(tta)_3(\mathbf{L})]\cdot CH_2Cl_2$ **Eu(t)**	$[Dy(tta)_3(\mathbf{L})]\cdot CH_2Cl_2$ **Dy(t)**	$[Dy(tta)_3(\mathbf{L})]$ **Dy(m)**
Formula	$C_{45}H_{28}Cl_2EuF_9N_2O_6S_{10}$	$C_{45}H_{28}Cl_2DyF_9N_2O_6S_{10}$	$C_{44}H_{26}DyF_9N_2O_6S_{10}$
M / g.mol^{-1}	1407.15	1417.69	1332.80
Crystal system	Triclinic	Triclinic	Monoclinic
Space group	P-1 (N°2)	P-1 (N°2)	$P2_1/a$
Cell parameters	a = 11.7393(7) Å b = 14.6701(9) Å c = 17.5396(9) Å α = 98.076(3) ° β = 101.888(3) ° γ = 113.182(2) °	a = 11.8296(17) Å b = 14.6040(3) Å c = 17.5490(3) Å α = 97.487(8) ° β = 102.277(7) ° γ = 113.599(7) °	a = 11.9987(32) Å b = 26.1502(60) Å c = 18.4103(44) Å β = 92.8746(98) °
Volume / Å^3	2633.4(3)	2634.8(7)	5769.3(35)
Z	2	2	4
T / K	150 (2)	150(2)	150(2)
2θ range /°	2.44 ≤ 2θ ≤ 55.22	5.88≤ 2θ ≤ 54.96	2.22≤ 2θ ≤ 54.96
ρ_{calc} / g.cm^{-3}	1.775	1.787	1.539
μ / mm^{-1}	1.770	1.997	1.729
Number of reflections	25495	30023	33108
Independent reflections	11896	12004	13110
R_{int}	0.0785	0.0448	0.1469
$Fo^2 > 2\sigma(Fo)^2$	5347	8894	3808
Number of variables	635	676	616
R_1, wR_2	0.0907, 0.2306	0.0621, 0.1666	0.0990, 0.2523

Compounds	$[Y(tta)_3(\mathbf{L})]$ **Y(m)**
Formula	$C_{44}H_{26}YF_9N_2O_6S_{10}$
M / g.mol^{-1}	1259.18
Crystal system	Monoclinic
Space group	$P2_1/a$
Cell parameters	a = 11.819(9) Å b = 26.130(20) Å c = 18.549(17) Å β = 93.280(30) °
Volume / Å^3	5719.0(90)
Z	4
T / K	150(2)
2θ range /°	2.20≤ 2θ ≤ 55.46
ρ_{calc} / g.cm^{-3}	1.463
μ / mm^{-1}	1.458
Number of reflections	36978
Independent reflections	12838
R_{int}	0.1406
$Fo^2 > 2\sigma(Fo)^2$	3881
Number of variables	620
R_1, wR_2	0.0938, 0.2395

Table S2. Selected bond lengths and angles for **Dy(t)** and **Dy(m)**.

	Dy(t)	**Dy(m)**
Dy-N1	2.575(5)	2.557(11)
Dy-N2	2.591(5)	2.631(12)
Dy-O1	2.339(5)	2.295(9)
Dy-O2	2.350(5)	2.341(9)
Dy-O3	2.304(5)	2.327(9)
Dy-O4	2.286(5)	2.316(9)
Dy-O5	2.348(5)	2.344(10)
Dy-O6	2.336(4)	2.330(10)

Table S3. SHAPE analysis of the coordination polyhedron around the lanthanide ions in complexes **Dy(t)** and **Dy(m)**.

Compound	$CShM_{SAPR-8}$ (square antiprism) D_{4d}	$CShM_{BTPR-8}$ (biaugmented trigonal prism) C_{2v}	$CShM_{TDD-8}$ (triangular dodecahedron) D_{2d}
Dy(t)	1.140	1.963	1.173
Dy(m)	0.808	2.193	2.531

Table S4. Oxidation potentials (V *vs* SCE, 0.1 M nBu_4NPF_6, in CH_2Cl_2 at 100 $mV.s^{-1}$) of the ligand **L** and related complexes.

	$E^1_{1/2}$	$E^2_{1/2}$
L	0.507	0.898
Eu(t)	0.522	0.911
Dy(m)	0.522	0.916
Y(m)	0.525	0.928

Table S5. Computed energies levels (the ground state is set at zero), component values of the Lande factor *g* and wavefunction composition for each M_J state of the ground-state multiplet for **Dy(t)** and **Dy(m)**.

	Energy (K)	g_x	g_y	g_z	Wavefunction composition
					Dy(t)
1	0.0	0.00	0.00	19.56	0.94 |±15/2>
2	225.9	0.10	0.11	16.31	0.81|±13/2> + 0.16|±9/2>
3	362.0	0.86	0.92	12.80	0.56 |±11/2> + 0.27 |±7/2>
4	447.2	3.27	4.18	8.92	0.38 |±5/2> + 0.27 |±9/2> + 0.10 |±3/2>
5	492.8	0.60	4.57	10.83	0.29 |±3/2> + 0.29 |±1/2> + 0.14 |±9/2>
6	541.6	2.72	4.11	12.37	0.30 |±5/2> + 0.23 |±3/2> + 0.21 |±7/2> + 0.15 |±1/2>
7	599.4	0.62	1.85	17.69	0.45 |±1/2> + 0.31 |±3/2> + 0.15 |±5/2>
8	787.0	0.01	0.02	19.71	0.28 |±9/2> + 0.23 |±7/2> + 0.21 |±11/2> + 0.13 |±5/2>
					Dy(t)
1	0.0	0.01	0.02	19.44	0.93 |±15/2>
2	197.0	0.25	0.47	15.38	0.70|±13/2> + 0.22|±9/2>
3	297.5	0.36	0.72	12.04	0.49 |±11/2> + 0.32 |±7/2>
4	380.1	2.14	3.75	9.25	0.35 |±5/2> + 0.21 |±9/2> + 0.14 |±13/2>
5	437.3	0.29	3.98	9.14	0.36 |±3/2> + 0.26 |±1/2> + 0.11 |±7/2> + 0.10 |±11/2>
6	493.5	2.26	5.35	13.02	0.25 |±5/2> + 0.22 |±7/2> + 0.16 |±3/2> + 0.16 |±1/2> + 0.14 |±9/2>
7	607.5	0.22	0.56	19.11	0.39 |±1/2> + 0.31 |±3/2> + 0.18 |±5/2>
8	718.0	0.02	0.04	19.71	0.27 |±9/2> + 0.25 |±11/2> + 0.19 |±7/2> + 0.10 |±5/2>

Table S6. Best fitted parameters (χ_T, χ_S, τ and α) with the extended Debye model for **Dy(t)** at 0 Oe in the temperature range 2-18 K.

T / K	χ_T / cm^3 mol^{-1}	χ_S / cm^3 mol^{-1}	α	τ / s	R^2
2	5.85625	0.2167	0.22926	0.00508	0.99926
2.2	5.39416	0.19371	0.23097	0.00506	0.99924
2.4	4.91494	0.18364	0.23087	0.00505	0.99923
2.6	4.53815	0.16434	0.23205	0.00502	0.99923
2.8	4.21537	0.16087	0.23136	0.005	0.99923
3	3.94029	0.1533	0.2315	0.00498	0.99924
3.5	3.38495	0.13246	0.23325	0.00487	0.99919
4	2.96838	0.11983	0.2325	0.00476	0.99922
4.5	2.65023	0.10615	0.23206	0.00461	0.99902
5	2.38113	0.10798	0.22906	0.00451	0.99915
5.5	2.16771	0.09911	0.22775	0.00431	0.9991
6	1.98795	0.09973	0.22329	0.00411	0.99909
7	1.70411	0.09693	0.21052	0.0036	0.99907
8	1.48964	0.09091	0.19521	0.00299	0.99907
9	1.31984	0.08829	0.17564	0.0024	0.99912
10	1.18604	0.08457	0.15626	0.00189	0.99925
11	1.07636	0.0795	0.13916	0.00145	0.99942
12	0.97882	0.07578	0.1226	0.00108	0.99958
13	0.9055	0.07048	0.11423	8.22E-04	0.99967
14	0.84251	0.068	0.1046	6.27E-04	0.99972
15	0.7872	0.06348	0.09922	4.75E-04	0.99979
16	0.7382	0.06499	0.09198	3.60E-04	0.99984
17	0.69518	0.06753	0.08461	2.72E-04	0.99986
18	0.6578	0.0716	0.08069	2.00E-04	0.9999

Table S7. Best fitted parameters (χ_T, χ_S, τ and α) with the extended Debye model for **Dy(m)** at 0 Oe in the temperature range 2-19 K.

T / K	χ_T / cm^3 mol^{-1}	χ_S / cm^3 mol^{-1}	α	τ / s	R^2
2	5.58038	0.27172	0.33481	0.00203	0.99932
2.2	5.1363	0.27543	0.33185	0.00204	0.99937
2.4	4.68683	0.25329	0.33293	0.00203	0.99932
2.6	4.32422	0.23724	0.33104	0.00201	0.99936
2.8	4.0191	0.21747	0.33138	0.00199	0.99936
3	3.75784	0.20786	0.33224	0.00199	0.99932
3.5	3.22697	0.1916	0.32965	0.00192	0.9994
4	2.82954	0.18007	0.32654	0.00189	0.99936
4.5	2.52809	0.12877	0.33055	0.00176	0.99913
5	2.26717	0.16119	0.31616	0.00177	0.99938
5.5	2.06294	0.14655	0.31072	0.00166	0.99934
6	1.8925	0.13736	0.3054	0.00155	0.99934
7	1.6209	0.12719	0.2878	0.0013	0.99939
8	1.41875	0.10699	0.28001	0.00101	0.99947
9	1.25773	0.09092	0.27192	7.54E-04	0.99954
10	1.1332	0.07388	0.27256	5.40E-04	0.99949
11	1.03056	0.07069	0.27624	3.94E-04	0.99951
12	0.93875	0.08202	0.27225	2.86E-04	0.99939
13	0.87085	0.09869	0.27292	2.23E-04	0.99942
14	0.80867	0.12581	0.26068	1.80E-04	0.99951

Table S8. Best fitted parameters (χ_T, χ_S, τ and α) with the extended Debye model for **Dy(t)** at 1 kOe in the temperature range 7-18 K.

T / K	χ_T / cm^3 mol^{-1}	χ_S / cm^3 mol^{-1}	α	τ / s	R^2
7	1.66312	0.04905	0.12408	0.0864	0.99985
8	1.44001	0.04616	0.10512	0.03678	0.99991
9	1.27179	0.04493	0.09305	0.01738	0.99986
10	1.14282	0.04289	0.0877	0.00904	0.99984
11	1.03787	0.04099	0.08354	0.00505	0.99989
12	0.94543	0.03786	0.08487	0.00285	0.99987
13	0.87554	0.0389	0.08319	0.0018	0.99986
14	0.81492	0.03837	0.08523	0.00118	0.99987
15	0.76198	0.03873	0.08413	7.88E-04	0.99986
16	0.71491	0.04192	0.0818	5.40E-04	0.99987
17	0.6765	0.04384	0.08112	3.71E-04	0.99988
18	0.63916	0.04922	0.07158	2.54E-04	0.9999

Table S9. Best fitted parameters (χ_T, χ_S, τ and α) with the extended Debye model for **Dy(m)** at 1 kOe in the temperature range 4.5-16 K.

T / K	χ_T / cm^3 mol^{-1}	χ_S / cm^3 mol^{-1}	α	τ / s	R^2
4.5	2.09766	0.08872	0.26459	0.11826	0.9995
5	1.95422	0.07624	0.27009	0.07146	0.99943
5.5	1.83319	0.06441	0.27733	0.04548	0.99914
6	1.75006	0.0527	0.29418	0.03083	0.99868
7	1.59575	0.03104	0.31945	0.0149	0.99835
8	1.42924	0.01481	0.32742	0.00715	0.99879
9	1.276	0.00522	0.3286	0.00352	0.99911
10	1.14844	0.00209	0.32525	0.00189	0.99911
11	1.04451	3.19E-14	0.32953	1.04E-03	0.99906
12	0.94868	0.00606	0.32508	5.83E-04	0.99904
13	0.8757	0.03021	0.31754	3.87E-04	0.99909
14	0.81372	0.05865	0.30507	2.71E-04	0.99917
15	0.75907	0.10724	0.28035	2.12E-04	0.9993
16	0.70758	0.14747	0.24995	1.69E-04	0.99957

Table S10. Best fitted parameters (χ_T, χ_S, τ and α) with the extended Debye model for **^{164}Dy(m)** at 0 kOe in the temperature range 2-12 K.

T / K	χ_T / cm^3 mol^{-1}	χ_S / cm^3 mol^{-1}	α	τ / s	R^2
2	5.46402	0.70549	0.31546	0.00338	0.99946
2.2	4.99459	0.67833	0.31488	0.00336	0.99951
2.4	4.58024	0.63869	0.31522	0.00333	0.99952
2.6	4.24113	0.60994	0.31494	0.00329	0.99953
2.8	3.95138	0.58136	0.31476	0.00325	0.99953
3	3.70203	0.55412	0.31574	0.0032	0.99953
3.5	3.19235	0.5015	0.31266	0.00306	0.99951
4	2.80958	0.46012	0.30681	0.00292	0.99947
4.5	2.50325	0.42637	0.29748	0.00274	0.9994
5	2.25883	0.40293	0.28278	0.00253	0.99936
5.5	2.05294	0.3825	0.26229	0.00229	0.99937
6	1.8813	0.36294	0.24324	0.00203	0.99937
7	1.61075	0.32376	0.20896	0.00149	0.99955
8	1.40942	0.28582	0.18644	0.00103	0.99974
9	1.25223	0.25144	0.1742	6.93E-04	0.99986
10	1.12963	0.22124	0.17335	4.57E-04	0.99987
11	1.02789	0.20084	0.1754	3.03E-04	0.99992
12	0.93889	0.18644	0.17854	2.01E-04	0.9999

Table S11. Best fitted parameters (χ_T, χ_S, τ and α) with the extended Debye model for **^{164}Dy(m)** at 1 kOe in the temperature range 4-13 K.

T / K	χ_T / cm^3 mol^{-1}	χ_S / cm^3 mol^{-1}	α	τ / s	R^2
4	2.79735	0.35163	0.27142	0.18566	0.99926
4.5	2.44601	0.32053	0.24806	0.09289	0.9998
5	2.2024	0.29306	0.23531	0.0519	0.99988
5.5	2.00396	0.27072	0.22478	0.03078	0.99983
6	1.84322	0.24921	0.21912	0.01918	0.99989
7	1.5903	0.22253	0.20995	0.00831	0.99987
8	1.3986	0.19315	0.2064	0.00395	0.99993
9	1.2478	0.17346	0.20611	0.00202	0.99993
10	1.12721	0.15582	0.21255	0.00108	0.99987
11	1.02919	0.14236	0.21698	6.11E-04	0.9999
12	0.93891	0.14103	0.22013	3.52E-04	0.99989
13	0.87002	0.13971	0.22105	2.22E-04	0.9999

Table S12. Best fitted parameters (χ_T, χ_S, τ and α) with the extended Debye model for **$Dy_{0.02}Y_{0.98}$(m)** at 0 kOe in the temperature range 4-18 K.

T / K	χ_T / cm^3 mol^{-1}	χ_S / cm^3 mol^{-1}	α	τ / s	R^2
4	0.06373	0.00807	0.44269	3.13692	0.9973
4.5	0.05129	0.00798	0.37799	1.07695	0.99342
5	0.04228	0.00836	0.28751	0.44029	0.99779
5.5	0.03796	0.00836	0.23883	0.24168	0.99793
6	0.03469	0.00831	0.2054	0.14315	0.9982
7	0.03035	0.00816	0.17203	0.05921	0.99868
8	0.02705	0.00801	0.13668	0.0274	0.99889
9	0.02494	0.00778	0.13039	0.01434	0.99888
10	0.02309	0.00781	0.12545	0.00784	0.99854
11	0.02149	0.00776	0.11787	4.59E-03	0.99886
12	0.02022	0.00747	0.124	2.57E-03	0.99905
13	0.01921	0.00769	0.10968	1.67E-03	0.99852
14	0.0183	0.00762	0.12428	1.10E-03	0.99896
15	0.01762	0.00762	0.10519	7.72E-04	0.99937
16	0.01684	0.00719	0.13967	5.09E-04	0.99906
17	0.01639	0.0077	0.12092	3.69E-04	0.9991
18	0.01577	0.00807	0.07833	2.74E-04	0.9977

Table S13. Best fitted parameters (χ_T, χ_S, τ and α) with the extended Debye model for **$Dy_{0.02}Y_{0.98}$(m)** at 1 kOe in the temperature range 4-18 K.

T / K	χ_T / cm^3 mol^{-1}	χ_S / cm^3 mol^{-1}	α	τ / s	R^2
4	0.05613	0.00581	0.24095	5.41686	0.99774
4.5	0.0455	0.00579	0.19991	1.88821	0.99496
5	0.04016	0.00568	0.17563	0.8533	0.99916
5.5	0.03612	0.00564	0.15182	0.42957	0.99932
6	0.03306	0.00567	0.13009	0.2365	0.9995
7	0.02994	0.00552	0.11125	0.08841	0.9977
8	0.02686	0.00551	0.11582	0.03972	0.99826
9	0.02346	0.0054	0.09781	0.01772	0.99887
10	0.02161	0.00557	0.08565	0.00948	0.99905
11	0.01988	0.00548	0.06732	0.00537	0.99831
12	0.01851	0.0052	0.06478	0.00288	0.99877
13	0.0194	0.00596	0.08312	0.00176	0.99912
14	0.01841	0.00567	0.10162	0.00115	0.99902

15	0.01751	0.0065	0.04979	7.97E-04	0.99909
16	0.01681	0.00624	0.08397	5.36E-04	0.99879
17	0.01611	0.0058	0.09783	3.57E-04	0.99878
18	0.01552	0.00597	0.10169	2.28E-04	0.99908

Table S14. Cell parameters for **$^{164}Dy_{0.07}Y_{0.93}$(m)**.

Compounds	[$^{164}Dy_{0.02}Y_{0.98}(tta)_3$(**L**)] **$^{164}Dy_{0.02}Y_{0.98}$(m)**
Formula M / g.mol^{-1}	$C_{44}H_{26}Y_{0.98}Dy_{0.02}F_9N_2O_6S_{10}$ 1407.15
Crystal system	Monoclinic
Space group	/
Cell parameters	a = 11.9472(20) Å b = 25.9495(42) Å c = 18.4933(28) Å α = 90° β = 93.1124(83) ° γ = 90°
Volume / Å^3	5754.9(22)
Z	4
T / K	150 (2)

Table S15. Best fitted parameters (χ_T, χ_S, τ and α) with the extended Debye model for **$^{164}Dy_{0.07}Y_{0.93}$(m)** at 0 kOe in the temperature range 3.5-20 K.

T / K	χ_T / cm^3 mol^{-1}	χ_S / cm^3 mol^{-1}	α	τ / s	R²
3.5	0.28897	0.02135	0.53961	4.56019	0.99883
4	0.23746	0.02059	0.46937	1.7317	0.99867
4.5	0.19017	0.01945	0.39038	0.65295	0.99779
5	0.15959	0.01877	0.31411	0.3111	0.99823
5.5	0.14015	0.01778	0.25909	0.17565	0.99838
6	0.12613	0.0167	0.21999	0.1079	0.99863
7	0.10632	0.01475	0.16816	0.04706	0.99911
8	0.09231	0.01326	0.13582	0.02292	0.9993
9	0.08183	0.01187	0.12001	0.01209	0.99955
10	0.07414	0.01095	0.11132	0.00692	0.99959
11	0.06732	0.00972	0.10789	0.00406	0.99974
12	0.06136	0.00881	0.11189	0.00241	0.99963
13	0.05665	0.00837	0.1066	0.00157	0.9996
14	0.05272	0.00817	0.09962	0.00107	0.99974
15	0.04924	0.00775	0.09912	7.32E-04	0.99977

16	0.04624	0.00761	0.09637	5.12E-04	0.99984
17	0.0435	0.00763	0.09134	3.59E-04	0.99982
18	0.0411	0.00744	0.08613	2.44E-04	0.99986
19	0.03896	0.00838	0.07873	1.68E-04	0.99982
20	0.03697	0.01019	0.05207	1.18E-04	0.99992

Table S16. Best fitted parameters (χ_T, χ_S, τ and α) with the extended Debye model for **$^{164}Dy_{0.07}Y_{0.93}$(m)** at 1 kOe in the temperature range 4-20 K.

T / K	χ_T / cm^3 mol^{-1}	χ_S / cm^3 mol^{-1}	α	τ / s	R^2
4	0.20944	0.01982	0.23701	3.82753	0.99914
4.5	0.17448	0.01779	0.20736	1.49301	0.99759
5	0.15209	0.01664	0.1752	0.69605	0.99965
5.5	0.13651	0.01508	0.15912	0.36537	0.99924
6	0.12349	0.01432	0.13736	0.20728	0.99947
7	0.10497	0.01262	0.11532	0.07858	0.99952
8	0.09141	0.01157	0.10048	0.03456	0.99977
9	0.08136	0.01048	0.09587	0.01684	0.99979
10	0.07395	0.00903	0.10421	0.00892	0.99959
11	0.06706	0.00869	0.10297	0.00501	0.99972
12	0.061	0.00824	0.09775	0.00287	0.99981
13	0.05645	0.00795	0.09355	0.00184	0.99977
14	0.05253	0.00742	0.09966	0.0012	0.99974
15	0.04907	0.00732	0.09554	8.12971E-4	0.99979
16	0.04603	0.00696	0.09591	5.54472E-4	0.99981
17	0.04334	0.00737	0.08583	3.84809E-4	0.99986
18	0.04095	0.0076	0.08447	2.63957E-4	0.99989
19	0.0388	0.00868	0.06719	1.79732E-4	0.99989
20	0.03692	0.00953	0.05651	1.17876E-4	0.99994

Table S17. Best fitted parameters (χ_T, χ_S, τ and α) with the extended Debye model for **$^{164}Dy_{0.05}Eu_{0.95}$(t)** at 0 Oe in the temperature range 3-19 K.

T / K	χ_T / cm^3 mol^{-1}	χ_S / cm^3 mol^{-1}	α	τ / s	R^2
3	0.32745	0.0219	0.55768	4.7847	0.99849
3.5	0.2667	0.02239	0.48272	1.84518	0.99856
4	0.22131	0.02212	0.40882	0.79788	0.99833
4.5	0.19049	0.02128	0.34893	0.40333	0.99804
5	0.16857	0.02057	0.30179	0.2296	0.99833
5.5	0.15199	0.01964	0.26733	0.13965	0.9985
6	0.13881	0.01891	0.23997	0.08944	0.99871
7	0.12041	0.01701	0.21647	0.04145	0.99885
8	0.10519	0.01579	0.18671	0.02037	0.99914
9	0.09367	0.01519	0.16548	0.01087	0.99932
10	0.08471	0.01444	0.154	0.00616	0.99943
11	0.07749	0.01394	0.14533	0.00368	0.99947
12	0.07108	0.01348	0.13995	0.00222	0.99953
13	0.06609	0.0131	0.13782	0.00146	0.99965
14	0.0619	0.01346	0.1284	9.98E-04	0.99968
15	0.0596	0.01626	0.11156	7.11E-04	0.99971
16	0.05629	0.01632	0.09894	4.93E-04	0.99981
17	0.05343	0.01531	0.11818	3.37E-04	0.99977
18	0.05088	0.01823	0.07476	2.61E-04	0.99982
19	0.04849	0.01734	0.07153	1.69E-04	0.99992

Table S18. Best fitted parameters (χ_T, χ_S, τ and α) with the extended Debye model for **$^{164}Dy_{0.05}Eu_{0.95}$(t)** at 1 kOe in the temperature range 3-19 K.

T / K	χ_T / cm^3 mol^{-1}	χ_S / cm^3 mol^{-1}	α	τ / s	R^2
3.5	0.37304	0.01799	0.50097	53.16273	0.99714
4	0.20745	0.01846	0.38522	4.66489	0.99616
4.5	0.16482	0.01824	0.31121	1.47549	0.99588
5	0.14272	0.0181	0.26049	0.66428	0.99685
5.5	0.12779	0.01747	0.23079	0.34483	0.99733
6	0.11618	0.01704	0.2074	0.1951	0.9978
7	0.10143	0.01592	0.19252	0.07673	0.99819
8	0.0883	0.01526	0.16491	0.03302	0.99847
9	0.07872	0.01475	0.14752	0.01593	0.99904
10	0.07125	0.01424	0.13297	0.00841	0.99945
11	0.06523	0.01385	0.12484	0.00472	0.99956
12	0.05996	0.01366	0.11559	0.00274	0.99961
13	0.05588	0.0135	0.11563	0.00171	0.9997
14	0.05253	0.01354	0.10585	0.00116	0.99961
15	0.04937	0.01354	0.09962	7.82E-04	0.99981
16	0.04668	0.01313	0.09935	5.26E-04	0.9997
17	0.04429	0.01283	0.09459	3.67E-04	0.99976
18	0.04207	0.01503	0.05187	2.70E-04	0.99976
19	0.04014	0.01484	0.0596	1.78E-04	0.99973

Table S19. Dynamic parameters collected above 10 K for the five previously investigated compounds at zero external field and at 1 kOe.

Compound	τ_0 (s)	Δ (K)
Dy(m) 0 Oe	$1.0(1)\times10^{-5}$	42(2)
Dy(m) 1 kOe	$2.7(4)\times10^{-6}$	65(2)
Dy(t) 0 Oe	$1.1(2)\times10^{-5}$	57(3)
Dy(t) 1 kOe	$1.2(3)\times10^{-6}$	96(4)
^{164}Dy(m) 0 Oe	$8.4(2)\times10^{-6}$	41(2)
^{164}Dy(m) 1 kOe	$2.4(6)\times10^{-6}$	60(2)
$Dy_{0.02}Y_{0.98}$(m) 0 Oe	$4.5(7)\times10^{-6}$	76(2)
$Dy_{0.02}Y_{0.98}$(m) 1 kOe	$2.9(7)\times10^{-6}$	82(3)
$^{164}Dy_{0.07}Y_{0.93}$(m) 0 Oe	$3.2(6)\times10^{-6}$	82(3)
$^{164}Dy_{0.07}Y_{0.93}$(m) 1 kOe	$2.4(6)\times10^{-6}$	84(4)
$^{164}Dy_{0.05}Eu_{0.95}$(t) 0 Oe	$4.4(9)\times10^{-6}$	74(3)
$^{164}Dy_{0.05}Eu_{0.95}$(t) 1 kOe	$3.3(7)\times10^{-6}$	80(3)

References

1 A. I. Vooshin, N. M. Shavaleev, V. P. Kazakov, *J. Luminescence* 2000, **91**, 49.

2 R. D. McCullough, M. A. Petruska, J. A.; Belot, *Tetrahedron* 1999, **55**, 9979.

3 X. Wang, P. Rabbat, P. O'Shea, R. Tillyer, E. J. J. Grabowski, P. J. Reider, *Tetrahedron. Lett.* 2000, **41**, 4335.

4 X. Chen, F. J. Femia, J. W. Babich, J. Zubiet, *Inorg. Chim. Acta* 2001, **314**, 91.

5 SHELX97 - Programs for Crystal Structure Analysis (Release 97-2). Sheldrick, G. M. Institut für Anorganische Chemie der Universität, Tammanstrasse 4, D-3400 Göttingen, Germany, 1998. SIR97 – A. Altomare, M. C. Burla, M. Camalli, G. L. Cascarano, C. Giacovazzo, A. Guagliardi, A. G. G. Moliterni, G. Polidori, R. Spagna, *J. Appl. Cryst.* 1999, **32**, 115.

6 F. Aquilante, L. De Vico, N. Ferré, G. Ghigo, P.A. Malmqvist, P. Neogrady, T. Bondo Pedersen, M. Pitonak, M. Reiher, B. O. Roos, L. Serrano-Andrés, M. Urban, V. Veryazov, R. Lindh, *J. Comput. Chem.* 2010, **31**, 224.

7 B. O. Roos, P. R. Taylor, P. E. M. Siegbahn, *Chem. Phys.* 1980, **48**, 157.

8 P. A. Malmqvist, B. O. Roos, B. Schimmelpfennig, *Chem. Phys. Lett.* 2002, **357**, 230.

9 P. A. Malmqvist, B. O. Roos, *Chem. Phys. Lett.* 1989, **155**, 189.

10 L. F. Chibotaru, L. Ungur, A. Soncini, *Angew. Chem., Int. Ed.* 2008, **47**, 4126.

11 F. Aquilante, P.-A. Malmqvist, T.-B. Pedersen, A. Ghosh, B. O. Roos, *J. Chem. Theory Comput.* 2008, **4**, 694.

12 B. O. Roos, R. Lindh, P.-A. Malmqvist, V. Veryazov, P.-O. Widmark, *J. Phys. Chem. A* 2004, **108**, 2851.

13 B. O. Roos, R. Lindh, P.-A.; Malmqvist, V. Veryazov, P.-O. Widmark, *J. Phys. Chem. A* 2005, **109**, 6576.

14 B. O. Roos, R. Lindh, P.-A. Malmqvist, V. Veryazov, P.-O. Widmark, A. C. Borin, *J. Phys. Chem. A* 2008, **112**, 11431.